Electroweak-correction effects in gauge-boson pair production at the LHC

E. ACCOMANDO[1], A. DENNER[1] AND S. POZZORINI[1,2]

[1] *Paul Scherrer Institut*
CH-5232 Villigen PSI, Switzerland

[2] *Institute of Theoretical Physics*
University of Zürich, Switzerland

Abstract:

We have studied the effect of one-loop logarithmic electroweak radiative corrections on WZ and Wγ production processes at the LHC. We present analytical results for the leading-logarithmic electroweak corrections to the corresponding partonic processes $\bar{\mathrm{d}}\mathrm{u} \to$ WZ, Wγ. Using the leading-pole approximation we implement these corrections into Monte Carlo programs for pp $\to l\nu_l l'\bar{l}', l\nu_l\gamma$. We find that electroweak corrections lower the predictions by 5–20% in the physically interesting region of large transverse momentum and small rapidity separation of the gauge bosons.

October 2001

1   Introduction

Vector-boson pair production provides us with an important testing ground for the non-abelian structure of the Standard Model (SM). While gauge-boson properties, such as masses and couplings to fermions, have already been measured with great accuracy at LEP and Tevatron, vector-boson self-interactions have not been tested with comparable precision. New physics occurring at energy scales much larger than those probed directly at forthcoming experiments could modify the structure of these interactions. These modifications are parametrized in terms of anomalous couplings in the Yang–Mills vertices.

In the last few years, the contribution of trilinear gauge-boson couplings was directly measured via vector-boson pair production at LEP2 and Tevatron. While, in particular, LEP2 has been able to produce W^+W^- pairs with high statistics, nevertheless all these events were generated at rather modest centre-of-mass (CM) energies ($E_{CM} \lesssim 210\,\mathrm{GeV}$). The effect of anomalous couplings is, on the other hand, expected to be strongly enhanced by increasing the invariant mass of the gauge-boson pair $M_{VV'}$ ($V, V' = \mathrm{W}, \mathrm{Z}, \gamma$), since these couplings in general spoil the unitarity cancellations for longitudinal gauge bosons. Hence, at future colliders it will be useful to analyse the di-boson production at the highest possible CM energies.

Moreover, vector-boson pairs constitute a background to other kinds of new-physics searches. One of the gold-plated signals for supersymmetry at hadron colliders is chargino–neutralino pair production, which would give rise to final states with three charged leptons and missing transverse momentum [1]; the primary background to this signature is given by WZ or $\mathrm{W}\gamma^*$ production. Leptonic final states, coming from WZ or $\mathrm{W}\gamma^*$, could also fake WZ vector-boson scattering signals, or $W^\pm W^\mp$ and $W^\pm W^\pm$ scattering signals if one of the charged leptons is lost in the beam pipe, which are again expected to be enhanced at high CM energies [2].

In the next years, hadron colliders will be the main source of vector-boson pairs with large invariant masses $M_{VV'}$. Tevatron Run II will collect from tens to hundreds of events, depending on the particular process. The large Hadron Collider (LHC) will further increase the event number by roughly two orders of magnitude [3]. Owing to the expected increase in statistics, theoretical predictions must reach high accuracy to allow for a decent analysis of the data.

Hadronic di-boson production has received a lot of attention (for a review on the subject see Ref. [3]). Originally computed by treating W and Z bosons as stable particles, tree-level cross sections for W^+W^-, $W^\pm\mathrm{Z}$, ZZ, $W^\pm\gamma$, and $\mathrm{Z}\gamma$ production and decay have been updated by evaluating, in narrow-width approximation but retaining spin information via decay-angle correlations, the doubly-resonant contribution to the four-fermion final states (e.g. $q\bar{q}' \to W^\pm\mathrm{Z} \to 4f$) [4] and the resonant contribution to two-fermion plus photon final states (e.g. $q\bar{q}' \to W^\pm\gamma \to 2f + \gamma$) [5]. As a further step, in the last few years Monte Carlo programs [6] have included the full $q\bar{q}' \to 4f$ amplitude, by taking into account finite-width effects and the irreducible background owing to non-doubly-resonant diagrams.

The $\mathcal{O}(\alpha_s)$ QCD corrections to gauge-boson pair-production and decay have been extensively analysed by many authors. Gauge-boson pair-production cross sections have been calculated at next-to-leading order (NLO) accuracy retaining the full spin corre-

lations of the leptonic decay products. Several NLO Monte Carlo programs have been implemented and cross checked so that complete $\mathcal{O}(\alpha_s)$ corrections are now available [4–6]. QCD corrections turn out to be quite significant at LHC energies. They can increase the lowest-order cross section by a factor two if no cuts are applied and by one order of magnitude for large transverse momentum or large invariant mass of the vector bosons [7,8]. By including a jet veto, their effects can be drastically reduced to the order of tens of per cent [9,4], but in any case they have to be considered to get realistic and reliable estimates of total cross sections and distributions.

In view of the envisaged precision of a few per cent at the LHC, also a discussion of electroweak corrections is in order. For single W- and Z-boson production, $\mathcal{O}(\alpha)$ corrections have been computed taking into account the full QED and weak contributions [10]. For gauge-boson pair production at hadron colliders, the electroweak corrections have been taken into account only via an effective mixing angle.

As well known, the impact of $\mathcal{O}(\alpha)$ electroweak contributions grows with increasing energy. Analyses of the high-energy behaviour of electroweak corrections in general and for specific e^+e^- and $\gamma\gamma$ processes have already been performed revealing effects which should be clearly visible at future linear colliders (see for instance Refs. [11,12]). At high energies the electroweak corrections are dominated by double and single logarithms of the ratio of the energy to the electroweak scale. In Refs. [13,14] it has been shown that the leading-logarithmic one-loop corrections to arbitrary electroweak processes factorize into the tree-level amplitudes times universal correction factors. These results represent a process-independent recipe for the calculation of leading logarithmic corrections.

Using the method of Refs. [13,14], we investigate in this paper the effect of leading-logarithmic electroweak corrections to the hadronic production of $W^\pm Z$ and $W^\pm\gamma$ pairs in the large-invariant-mass region of the hard process at the LHC. Since the aim of this paper is to describe the structure of the $\mathcal{O}(\alpha)$ electroweak corrections and to give an estimate of their size, we have not included QCD corrections. Also, QED corrections are not fully considered as they strictly depend on the experimental setup. We omit all infrared-singular terms originating from the massless photon, as explained in App. A.1 and focus on the contributions of the leading electroweak logarithms originating from above the electroweak scale.

The simplest experimental analyses of gauge-boson pair production will rely on purely leptonic final states. Semi-leptonic channels, where one of the vector bosons decays hadronically, have been analysed at the Tevatron [15] showing that these events suffer from the background due to the production of one vector boson plus jets via gluon exchange. For this reason, we choose to analyse only di-boson production where both gauge bosons decay leptonically into e or μ.

The paper is organized as follows: in Sect. 2 we give some details on the general setup of our calculation. In Sect. 3 and App. A the logarithmic electroweak one-loop corrections are examined and presented in analytical form. Section 4 contains a numerical discussion for WZ production and decay, while Sect. 5 covers Wγ production and decay. Our findings are summarized in Sect. 6.

2 Processes and their computation

We consider in detail two classes of processes,

(i) $pp \rightarrow l\nu_l l'\bar{l}'$, with $l, l' = e, \mu$, and

(ii) $pp \rightarrow l\nu_l\gamma$, with $l = e, \mu$.

The first class is characterized by three isolated charged leptons plus missing energy in the final state. In our notation, $l\nu_l$ indicates both $l^-\bar{\nu}_l$ and $l^+\nu_l$. This kind of processes includes WZ production as intermediate state. The second class is instead related to Wγ production. Both classes of processes are described by the formula

$$d\sigma^{h_1 h_2}(P_1, P_2, p_f) = \sum_{i,j} \int dx_1 dx_2 \; f_{i,h_1}(x_1, Q^2) f_{j,h_2}(x_2, Q^2) \, d\hat{\sigma}^{ij}(x_1 P_1, x_2 P_2, p_f), \quad (2.1)$$

where p_f summarizes the final-state momenta, f_{i,h_1} and f_{j,h_2} are the distribution functions of the partons i and j in the incoming hadrons h_1 and h_2 with momenta P_1 and P_2, respectively, Q is the factorization scale, and $\hat{\sigma}^{ij}$ represent the cross sections for the partonic processes. Since the two incoming hadrons are protons and we sum over final states with opposite charges, we find

$$
\begin{aligned}
d\sigma^{h_1 h_2}(P_1, P_2, p_f) = \int dx_1 dx_2 \sum_{U=u,c} \sum_{D=d,s} \Big[& f_{\bar{D},p}(x_1, Q^2) f_{U,p}(x_2, Q^2) \, d\hat{\sigma}^{\bar{D}U}(x_1 P_1, x_2 P_2, p_f) \\
+ & f_{\bar{U},p}(x_1, Q^2) f_{D,p}(x_2, Q^2) \, d\hat{\sigma}^{\bar{U}D}(x_1 P_1, x_2 P_2, p_f) \\
+ & f_{D,p}(x_1, Q^2) f_{\bar{U},p}(x_2, Q^2) \, d\hat{\sigma}^{D\bar{U}}(x_1 P_1, x_2 P_2, p_f) \\
+ & f_{U,p}(x_1, Q^2) f_{\bar{D},p}(x_2, Q^2) \, d\hat{\sigma}^{U\bar{D}}(x_1 P_1, x_2 P_2, p_f) \Big] \quad (2.2)
\end{aligned}
$$

in leading order of QCD.

The tree-level amplitudes for the partonic processes have been generated by means of PHACT [16], a set of routines based on the helicity-amplitude formalism of Ref. [17]. For the numerical results presented here, we have used the fixed-width scheme with $\Gamma_Z = 2.512\,\text{GeV}$ and $\Gamma_W = 2.105\,\text{GeV}$, and the input masses $M_Z = 91.187\,\text{GeV}$ and $M_W = 80.45\,\text{GeV}$. The weak mixing angle is fixed by $s_W^2 = 1 - M_W^2/M_Z^2$. Moreover, we adopted the so called G_μ-scheme, which effectively includes higher-order contributions associated with the running of the electromagnetic coupling and the leading universal two-loop m_t-dependent corrections. This corresponds to parametrize the lowest-order matrix element in terms of the effective coupling $\alpha_{G_\mu} = \sqrt{2}G_\mu M_W^2 s_W^2/\pi$. However, we use $\alpha(0) = 1/137.036$ for the coupling of the real photon in $pp \rightarrow l\nu_l\gamma$, i.e. we multiply the corresponding cross sections in the G_μ-scheme by $\alpha(0)/\alpha_{G_\mu}$. Additional input parameters are the quark-mixing matrix elements whose values have been taken to be $|V_{ud}| = |V_{cs}| = 0.975$, $|V_{us}| = |V_{cd}| = 0.222$, and zero for all other relevant matrix elements.

As to parton distributions, we have used CTEQ(5M1) [18] at the factorization scales

$$Q^2 = \frac{1}{2}\left(M_W^2 + M_Z^2 + P_T^2(l\nu_l) + P_T^2(l'\bar{l}')\right) \quad (2.3)$$

and

$$Q^2 = \frac{1}{2} \left(M_W^2 + P_T^2(l\nu_l) + P_T^2(\gamma) \right) \tag{2.4}$$

for WZ and Wγ production processes, respectively, where P_T denotes the transverse momentum. This scale choice appears to be appropriate for the calculation of differential cross sections, in particular for vector-boson transverse-momentum distributions [8,4].

We have, moreover, implemented a general set of cuts, proper for LHC analyses, defined as follows:

- lepton transverse momentum $P_T(l) > 20\,\text{GeV}$,

- missing transverse momentum $P_T^{\text{miss}} > 20\ (50)\,\text{GeV}$ for WZ (Wγ),

- lepton pseudo-rapidity $|\eta_l| < 3\ (2.5)$ for WZ (Wγ), where $\eta_i = -\log(\tan\theta_i/2)$, θ_i is the polar angle of particle i with respect to the beam, and $i = l, \gamma$,

- rapidity–azimuthal-angle separation $\Delta R_{l\gamma} = \sqrt{(\eta_l - \eta_\gamma)^2 + (\phi_l - \phi_\gamma)^2} > 0.7$ between charged lepton and photon for Wγ.

For the different processes considered, we have also used further cuts which are described in due time. In the following sections, we present results for the LHC at CM energy $\sqrt{s} = 14\,\text{TeV}$ and an integrated luminosity $L = 100\,\text{fb}^{-1}$.

3 Electroweak $\mathcal{O}(\alpha)$ corrections

We are interested in the electroweak $\mathcal{O}(\alpha)$ corrections to the processes $pp \to l\nu_l l'\bar{l}'$ and $pp \to l\nu_l\gamma$ in the region of phase space where these are dominated by the gauge-boson pair-production subprocesses $pp \to WZ$ and $pp \to W\gamma$, respectively. In this region, the dominant contributions are those that are enhanced by the resonant propagators of the W boson and in the first process also of the Z boson. These can be most effectively calculated in the so-called leading-pole approximation (LPA), which is a double-pole approximation (DPA) for $pp \to WZ \to l\nu_l l'\bar{l}'$ and a single-pole approximation (SPA) for $pp \to W\gamma \to l\nu_l\gamma$. The LPA has been successfully applied for the calculation of electroweak corrections to W-pair production [19–21].

At tree level, the DPA for the partonic process $qq' \to WZ \to l\nu_l l'\bar{l}'$ reads

$$\mathcal{M}_{\text{Born,DPA}}^{qq' \to WZ \to l\nu_l l'\bar{l}'} = \frac{\text{i}}{p_W^2 - M_W^2 + \text{i}M_W\Gamma_W} \frac{\text{i}}{p_Z^2 - M_Z^2 + \text{i}M_Z\Gamma_Z} \times \sum_{\lambda,\lambda'} \mathcal{M}_{\text{Born}}^{qq' \to W_\lambda Z_{\lambda'}} \mathcal{M}_{\text{Born}}^{W_\lambda \to l\nu_l} \mathcal{M}_{\text{Born}}^{Z_{\lambda'} \to l'\bar{l}'}, \tag{3.1}$$

where the gauge-dependent doubly-resonant contribution is replaced by the well-defined gauge-independent residue, and $\mathcal{M}_{\text{Born}}^{qq' \to W_\lambda Z_{\lambda'}}$, $\mathcal{M}_{\text{Born}}^{W_\lambda \to l\nu_l}$, and $\mathcal{M}_{\text{Born}}^{Z_{\lambda'} \to l'\bar{l}'}$ denote the on-shell Born matrix elements for the boson production and decay processes. The sum runs over the physical helicities $\lambda, \lambda' = 0, \pm 1$ of the on-shell projected W and Z bosons (see App. A

of Ref. [20] for details), while the momenta of the virtual W and Z bosons are denoted by p_W and p_Z, respectively. For the process $qq' \to W\gamma \to l\nu_l\gamma$, the SPA is given by

$$\mathcal{M}^{qq'\to W_{\lambda'}\gamma_{\lambda'}\to l\nu_l\gamma_{\lambda'}}_{\text{Born,SPA}} = \frac{i}{p_W^2 - M_W^2 + iM_W\Gamma_W} \sum_\lambda \mathcal{M}^{qq'\to W_\lambda\gamma_{\lambda'}}_{\text{Born}} \mathcal{M}^{W_\lambda\to l\nu_l}_{\text{Born}}. \qquad (3.2)$$

In LPA, the $\mathcal{O}(\alpha)$ electroweak corrections to boson-production processes can be divided into two classes, factorizable and non-factorizable corrections. The non-factorizable corrections, i.e. those contributions that cannot be associated with either boson production or decay, have been evaluated for boson-pair production in e^+e^- annihilation in Refs. [22,23]. There, these corrections turned out to be small. We assume that this holds as well for the similar processes considered here and do not consider non-factorizable corrections any further.

Moreover, we do not include real corrections and restrict our discussion to the infrared-finite part of the virtual factorizable corrections, as defined in App. A.1. These contributions can be expressed in terms of the corrections to the on-shell boson production and decay subprocesses. The matrix element for the virtual corrections to the process $qq' \to WZ \to l\nu_l l'\bar{l}'$ can be written as

$$\begin{aligned}
\delta\mathcal{M}^{qq'\to WZ\to l\nu_l l'\bar{l}'}_{\text{virt,DPA}} = {} & \frac{i}{p_W^2 - M_W^2 + iM_W\Gamma_W} \frac{i}{p_Z^2 - M_Z^2 + iM_Z\Gamma_Z} \\
& \sum_{\lambda,\lambda'} \Big\{ \delta\mathcal{M}^{qq'\to W_\lambda Z_{\lambda'}}_{\text{virt}} \mathcal{M}^{W_\lambda\to l\nu_l}_{\text{Born}} \mathcal{M}^{Z_{\lambda'}\to l'\bar{l}'}_{\text{Born}} \\
& + \mathcal{M}^{qq'\to W_\lambda Z_{\lambda'}}_{\text{Born}} \delta\mathcal{M}^{W_\lambda\to l\nu_l}_{\text{virt}} \mathcal{M}^{Z_{\lambda'}\to l'\bar{l}'}_{\text{Born}} \\
& + \mathcal{M}^{qq'\to W_\lambda Z_{\lambda'}}_{\text{Born}} \mathcal{M}^{W_\lambda\to l\nu_l}_{\text{Born}} \delta\mathcal{M}^{Z_{\lambda'}\to l'\bar{l}'}_{\text{virt}} \Big\},
\end{aligned} \qquad (3.3)$$

where $\delta\mathcal{M}^{qq'\to W_\lambda Z_{\lambda'}}_{\text{virt}}$, $\delta\mathcal{M}^{W_\lambda\to l\nu_l}_{\text{virt}}$, and $\delta\mathcal{M}^{Z_{\lambda'}\to l'\bar{l}'}_{\text{virt}}$ denote the virtual corrections to the on-shell matrix elements for the boson production and decay processes. A similar expression holds for the process $qq' \to W\gamma \to l\nu_l\gamma$.

We focus in particular on the corrections involving single and double enhanced electroweak logarithms at high energies, i.e. on $\mathcal{O}(\alpha)$ contributions proportional to $\alpha\log^2(\hat{s}/M_W^2)$ or $\alpha\log(\hat{s}/M_W^2)$, where $\sqrt{\hat{s}}$ is the CM energy of the partonic subprocess. The logarithmic approximation yields the dominant corrections at CM energies large compared to the gauge-boson masses, $\hat{s} \gg M_W^2$. In the high-energy limit, however, there might be also enhanced non-logarithmic contributions that are a priori relevant. In general they contain constant terms proportional to M_H^2/M_W^2 and m_t^2/M_W^2. While for transverse gauge bosons, these Higgs- and top-mass-dependent corrections are entirely due to renormalization effects and can be effectively accounted for by using the G_μ-scheme, for longitudinal gauge bosons additional contributions of this kind exist. These non-logarithmic $\mathcal{O}(\alpha)$ contributions are process-dependent. For $e^+e^- \to W^+W^-$, where complete $\mathcal{O}(\alpha)$ corrections and their high-energy limit are available [11], the above terms turn out to be of order of a few per cent. We can then qualitatively assume that this holds as well for similar processes like hadronic di-boson production, even if only an exact computation could really furnish a precise statement on this point. Neglecting non-logarithmic terms can therefore

be considered a reasonable approximation at the LHC, where the experimental accuracy in the high-energy regime is at the few-per-cent level.

Since the decay processes involve no large-energy variable, the corresponding virtual corrections vanish in the logarithmic approximation. As a consequence, we do not consider in the following the last two contributions on the right-hand side of (3.3). Moreover, for the boson production processes $qq' \to WZ, W\gamma$ we take into account only the correction to the dominating channels involving two transverse (TT) or two longitudinal (LL) gauge bosons. The contributions of the mixed (LT, TL) channels are suppressed relatively to the others by factors of $M_W/\sqrt{\hat{s}}$ in the high-energy limit (see Fig. 2), and thus the corresponding corrections are unimportant.

The logarithmic virtual electroweak corrections to the dominating channels are calculated using the general method given in Refs. [13,14]. The corresponding analytical expressions for the processes $\bar{d}u \to W_\lambda^+ N_\lambda$, $N = Z, \gamma$, are given in App. A. Those for $d\bar{u} \to W_\lambda^- N_\lambda$ are derived via CP symmetry [see (A.2)]. Our predictions are obtained by considering the matrix element squared

$$|\mathcal{M}|^2 = |\mathcal{M}_{\mathrm{Born}}|^2 + 2\,\mathrm{Re}\left[\mathcal{M}_{\mathrm{Born,LPA}}\delta\mathcal{M}_{\mathrm{virt,LPA}}^\dagger\right], \qquad (3.4)$$

where $\mathcal{M}_{\mathrm{Born}}$ is the exact Born amplitude, while the $\mathcal{O}(\alpha)$ contribution is computed in LPA based on (3.1)–(3.3), and the formulas given in App. A. In the high-energy limit, a reasonable approach is to neglect fermion and boson masses, as compared with $\sqrt{\hat{s}}$, wherever possible. The expressions given in App. A are based on this approximation. However, we take into account the exact kinematics by evaluating the complete four-fermion or two-fermion-plus-photon phase space and use the exact values of the kinematical invariants in all formulas. Moreover, we do not use the high-energy approximations (A.7) and (A.8) in the correction factors but we implement the $\mathcal{O}(\alpha)$ contributions according to the full expressions given in (A.12), (A.13), (A.18), and (A.21)–(A.23) with the exact (SU(2)-transformed) Born matrix elements. Owing to our choice of the input-parameter scheme, the terms proportional to $\Delta\alpha(M_W^2)$ in (A.22) and (A.23) are omitted, since these are already taken into account by using α_{G_μ} instead of $\alpha(0)$ as input.

In the universal logarithmic corrections given in App. A, the pure angular-dependent logarithms, such as $\alpha \log^2(|\hat{r}|/\hat{s})$ and $\alpha \log(|\hat{r}|/\hat{s})$ with $\hat{r}$ equal to the Mandelstam variables $\hat{t}$ and $\hat{u}$ of the partonic subprocess, are not included. The validity of this approximation relies therefore on the assumption that all the variables $\hat{s}$, $|\hat{t}|$, and $|\hat{u}|$ are large compared with M_W^2 and approximately of the same size,

$$\hat{s} \sim |\hat{t}| \sim |\hat{u}| \gg M_W^2. \qquad (3.5)$$

This implies that the produced gauge bosons have to be emitted at sufficiently large angles with respect to the beam. Hence, the validity range of the high-energy logarithmic approximation for the radiative corrections corresponds to the central region of the boson scattering angle in the di-boson rest-frame. For s-channel processes, integrating over the full angular domain does not affect the reliability of the result at logarithmic level, since the neglected pure angular-dependent logarithms would give rise only to subleading constant terms, if included. For t-channel dominated scatterings like WZ or Wγ production, the situation is instead more delicate. The t-channel pole in the Born matrix element

gives rise to additional enhanced logarithms when integrated over the full kinematical range. Since these terms are not included in our $\mathcal{O}(\alpha)$ analysis, we have to take care that we do not get sizeable contributions from small scattering angles with respect to the beam. On the other hand, our formulas do not fake spurious contributions as long as $\hat{s}, |\hat{t}|, |\hat{u}| \lll M_W^2$, since the large logarithms become small for $\hat{s}, |\hat{t}|, |\hat{u}| \sim M_W^2$.

4 W$^\pm$Z production

In this section, we present some cross sections and distributions for the leptonic processes $pp \rightarrow l\nu_l l'\bar{l}'$ with $l, l' = e, \mu$. These final states allow to analyse WZ production and thus in particular to test trilinear gauge-boson couplings. Systematic studies of the effect of anomalous couplings on the hadronic production of gauge-boson pairs have shown that deviations from the SM cross sections should be particularly enhanced when gauge bosons are produced at high CM energies and at large scattering angles in the di-boson rest-frame. The same kinematical region is also proper to search for scatterings of strongly interacting vector bosons.

It is therefore particularly interesting to study the electroweak corrections in these kinematical configurations, where their effect is also expected to be more sizeable. As an illustration of the behaviour and the size of the $\mathcal{O}(\alpha)$ contributions, we have chosen to analyse the distribution of the reconstructed Z-boson transverse momentum $P_T(l'\bar{l}')$. The P_T variable is commonly used at hadron colliders because large P_T requires high CM energies and large angles. We study also pure angular observables of interest in the high-energy regime of the hard scattering.

4.1 Born level

We start recalling basic properties of the Born amplitude, which are useful later in discussing radiative-correction effects. In Fig. 1, just for explicative purposes, we have plotted the on-shell Born cross section for the partonic process $\bar{d}u \rightarrow W^+Z$ as a function of the angle $\hat{\theta}$ between the $\bar{d}$ quark and the Z boson in the $\bar{d}u$ CM frame, at fixed energy $E_{CM} = 500 \, \text{GeV}$ and before any convolution with quark distribution functions. We have reported the different helicity contributions separately. As can be seen, the transverse component σ_{TT} shows the well-known radiation zero for $\cos\hat{\theta} = (g_{u,L} + g_{d,L})/(g_{u,L} - g_{d,L}) = -s_W^2/(3c_W^2) \approx -0.1$ [9], where $g_{u,L}$ and $g_{d,L}$ represent the Z-boson couplings to left-handed up and down quarks, respectively, and is strongly peaked in the forward and backward directions. The longitudinal contribution σ_{LL} is instead concentrated in the central region, at large angle of the Z-boson with respect to the incoming quarks. Integrating over the angle from 0° to 180°, one obtains the total cross sections shown in Fig. 2 (see the three curves on the left side) as a function of the energy. As expected, the dominant contribution is given by σ_{TT}, and above $300 \, \text{GeV}$ all polarized cross sections decrease with energy.

The behaviour of the polarized cross sections depends, however, on the selected kinematical region. If we consider the region of phase space characterized by a large transverse momentum of the Z boson, the relative size of the different helicity components and the
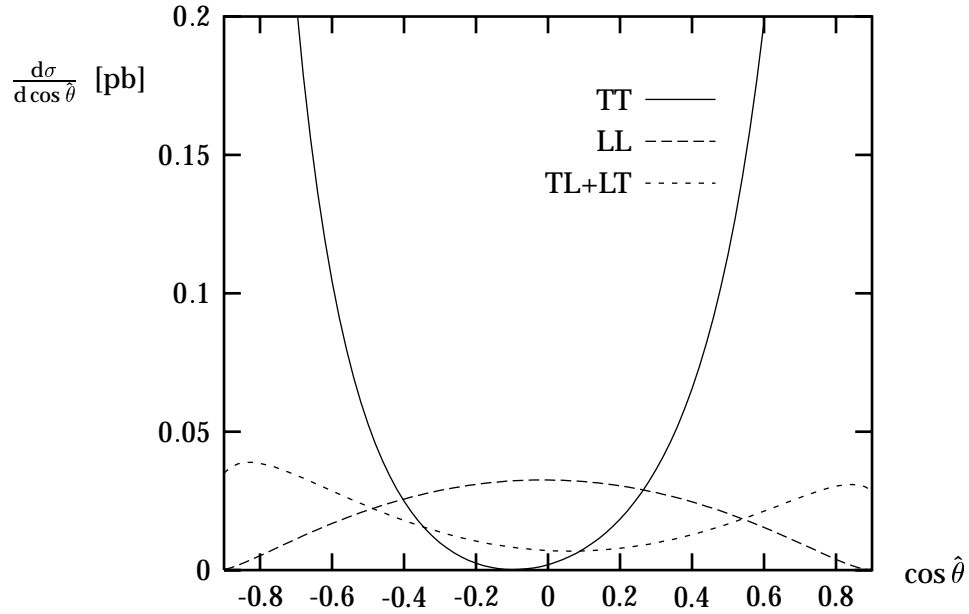
Figure 1: Lowest-order angular distributions for the process $\bar{\mathrm{d}}\mathrm{u} \to \mathrm{W}^+_\lambda \mathrm{Z}_{\lambda'}$ at $E_{\mathrm{CM}} = 500\,\mathrm{GeV}$. Here λ, λ' denote the transverse (T) or longitudinal (L) helicities.
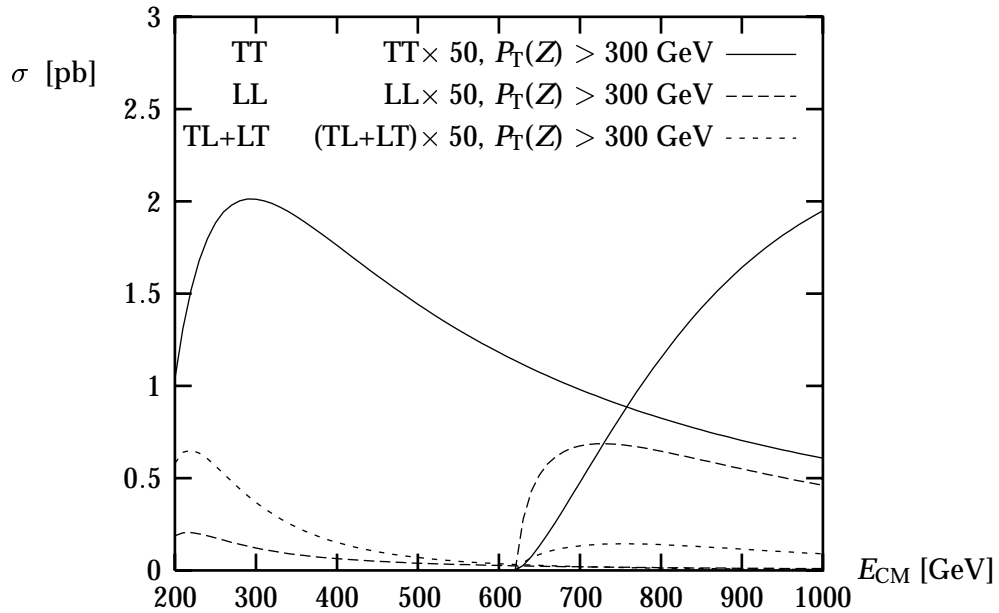
Figure 2: Born cross sections for the process $\bar{\mathrm{d}}\mathrm{u} \to \mathrm{W}^+_\lambda \mathrm{Z}_{\lambda'}$ as a function of E_{CM} with λ, λ' as in Fig. 1. From left to right, the three legends refer to the left-side curves and to the right-side ones respectively, as explained in the text.
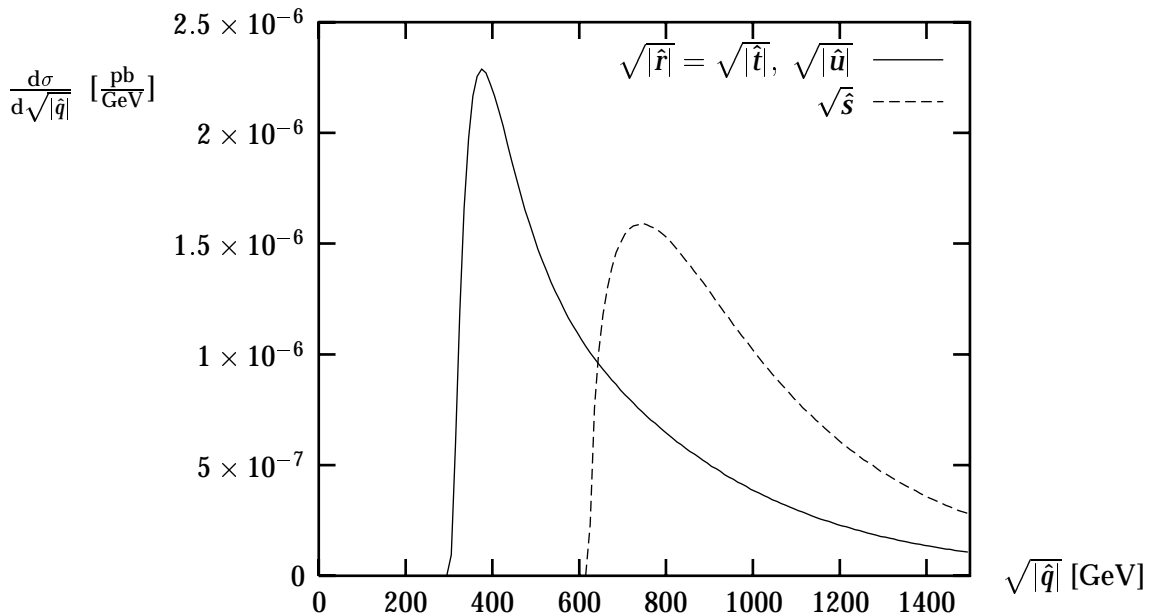
8

Figure 3: Lowest-order distributions in the invariants $\sqrt{\hat{s}}$ and $\sqrt{|\hat{r}|}$ as defined in the text for the full process $pp \to l\nu_l l'\bar{l}'$ at $\sqrt{s} = 14\,\text{TeV}$. Standard cuts and $P_\text{T}(l'\bar{l}') > 300\,\text{GeV}$ are applied.

shape of the curves change sensibly. As before, we plot the cross sections versus the CM energy but now for $P_\text{T}(Z) > 300\,\text{GeV}$ (see the three curves starting at around $600\,\text{GeV}$ in Fig. 2). In this case the LL contribution dominates at smaller energies, while the TT component increases with energy and takes over at high CM energies. This is due to the fact that the above-mentioned P_T cut translates into a minimum CM energy, $E_\text{CM} \simeq 624\,\text{GeV}$, and limits the allowed range of the scattering angle of the Z boson. Hence, at low energies, the allowed angular region is strictly central and the LL component dominates. At larger energies, the allowed kinematical range increases by including smaller angles, and the TT contribution rapidly grows, soon overwhelming the LL part.

Of course, one has to consider the additional effect due to the partonic distribution functions, which in turn decrease with increasing momentum fractions x_i and therefore with increasing CM energy $\sqrt{\hat{s}} = \sqrt{x_1 x_2 s}$. The net result is shown in Fig. 3, where the distribution in the hard-scattering energy $\sqrt{\hat{s}}$ is plotted. Here and in the following we consider the full process $pp \to 4f$, summed over all electron and muon final states, $e^{\pm}\overset{(-)}{\nu_e}e^+e^-$, $e^{\pm}\overset{(-)}{\nu_e}\mu^+\mu^-$, $\mu^{\pm}\overset{(-)}{\nu_\mu}e^+e^-$, and $\mu^{\pm}\overset{(-)}{\nu_\mu}\mu^+\mu^-$. We have moreover applied our standard cuts as defined in Sect. 2 and the additional cut $P_\text{T}(l'\bar{l}') > 300\,\text{GeV}$ on the reconstructed Z boson. As can be seen, despite the suppression resulting from the decrease of the parton distributions with energy, roughly 50% of the contribution to the total cross section comes from the high-energy region $\sqrt{\hat{s}} > 1\,\text{TeV}$. We come back to this point later when discussing radiative corrections.

As explained in Sect. 3, the DPA has proven to be a powerful tool for the computation of radiative corrections. In order to analyse, for the process considered here, the appli-
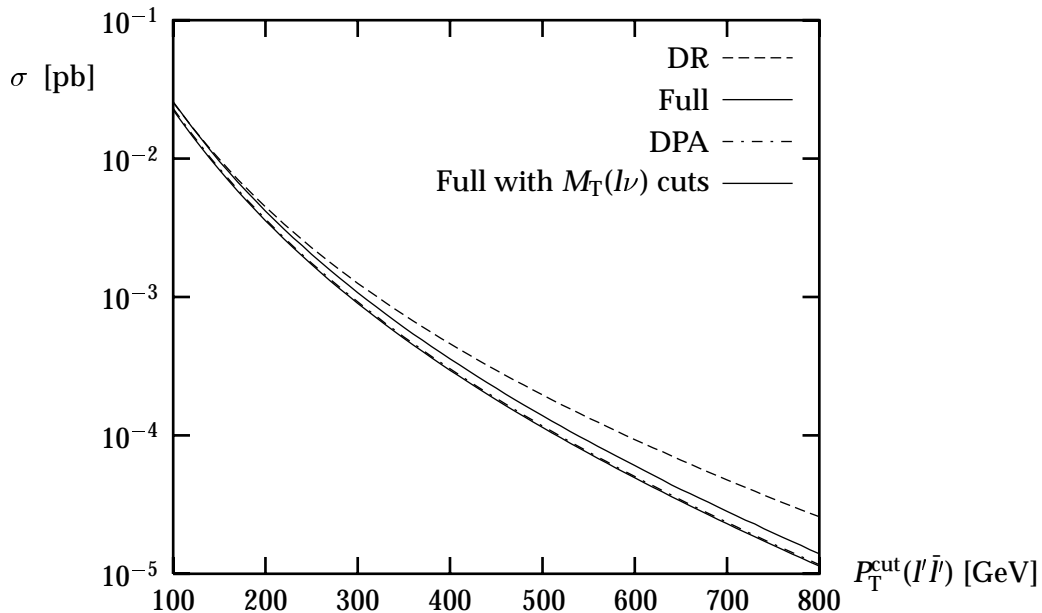
9

Figure 4: Born cross section for the full process $pp \to l\nu_l l'\bar{l}'$ at $\sqrt{s} = 14\,\text{TeV}$ as a function of the cut on the transverse momentum of the reconstructed Z boson. Standard cuts are applied.

cability of this approximation in a wide range of energies, we have plotted in Fig. 4 the tree-level cross section as a function of the $P_\text{T}(l'\bar{l}')$ cut. The first three curves represent, from top to bottom, the contribution of the pure doubly-resonant (DR) diagrams, the full result including all Feynman diagrams which contribute to the same final state (the number of diagrams is 10 in absence of identical particles in the final state, otherwise it doubles), and finally the DPA as defined in (3.1).

If one looks at the difference between the complete result and the DPA, one can see that the discrepancy is rather remarkable. It amounts in fact to roughly 15% for $P_\text{T}(l'\bar{l}')$ cuts above $100\,\text{GeV}$. Let us note that, for this process, the commonly adopted narrow-width approximation, which corresponds to *production* $\times$ *decay*, differs from the DPA by less than 2% for the considered range of $P_\text{T}^\text{cut}(l'\bar{l}')$. So, depending on applied cuts and selected energy range, the narrow-width approximation can underestimate the exact result by roughly 13%. This points out the need of using the exact matrix element at lowest order, as specified in (3.4).

The second information one can extract from Fig. 4 is related to the contribution of non-DR diagrams. As shown by the dashed-line, the DR contribution ($pp \to WZ \to 4f$), which is lower than the exact result by about 1% around threshold, increases with energy relatively to the full result. For $P_\text{T}^\text{cut}(l'\bar{l}') = 300\,\text{GeV}$, the difference between the two cross sections is already of order 20%, and at very large energies the DR diagrams can even overestimate the result by a factor 2 or more. This effect is due to delicate gauge cancellations between DR and non-DR diagrams, which characterize the behaviour of off-shell cross sections in the high-energy regime. DR and non-DR diagrams do not constitute two separately gauge-independent subsets. Hence, the pure DR contribution cannot be
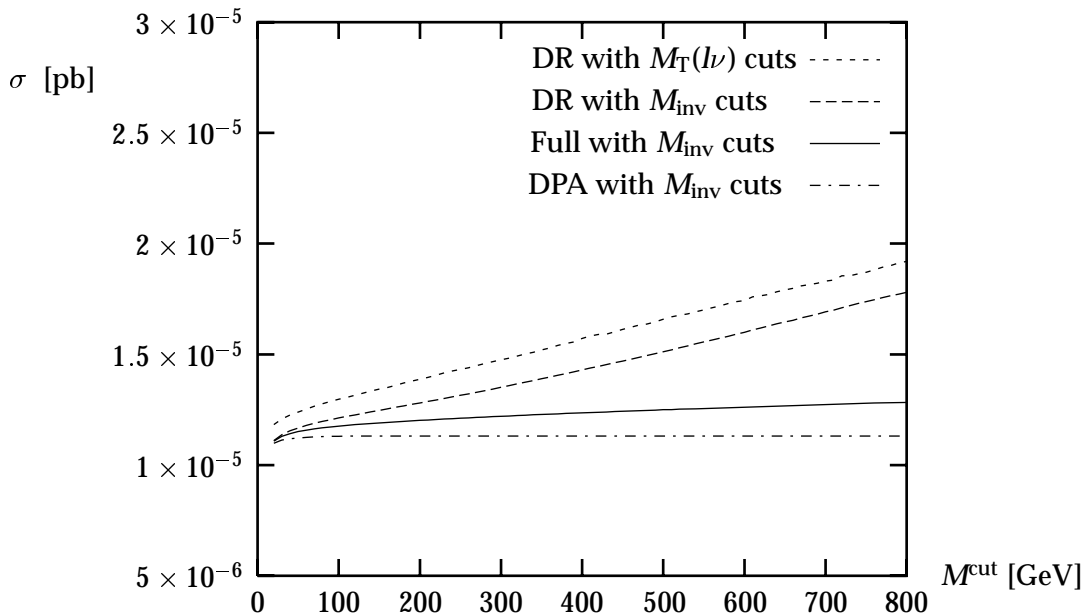
10

Figure 5: Born cross section for the process $pp \to l\nu_l l'\bar{l}'$ at $\sqrt{s} = 14\,\mathrm{TeV}$ as a function of the upper cut M^{cut} on the two invariant masses, $M(ij)$, of the leptonic pairs which could reconstruct W and Z bosons, as explained in the text. Standard cuts and $P_{\mathrm{T}}(l'\bar{l}') > 800\,\mathrm{GeV}$ are applied.

considered as a physical observable and the signal definition based on the diagrammatic approach and commonly adopted for example at LEP2 for WW and ZZ physics is not anymore adequate to describe di-boson production at the LHC in the high-P_{T} region. The only sensible observable is the total contribution or the DPA which is a well-defined gauge-independent quantity.

In order to investigate whether the difference between DR and full result is essentially due to the off-shellness of the gauge bosons as expected, we have then studied the effects of possible kinematical cuts. In Fig. 5, we have plotted the cross section for the extreme case $P_{\mathrm{T}}(l'\bar{l}') = 800\,\mathrm{GeV}$ as a function of an upper cut M^{cut} applied on the two invariant masses $M(ij)$ of the leptonic pairs which could reconstruct the Z and W bosons, $M(ij) < M_V + M^{\mathrm{cut}}$. We assume a lower cut $M(ij) > M_V - 20\,\mathrm{GeV}$, which is kept fixed in order to suppress the contribution from the virtual photon. As can be seen, for $M^{\mathrm{cut}} = 20\,\mathrm{GeV}$ the difference between DR and the exact result reduces to the per-cent level. Also, both converge towards the DPA value, represented by the nearly flat dot-dashed line. It is quite obvious that cross sections computed in DPA are not sensible to this kind of cuts, as the gauge bosons are always considered on-shell except for the weakly cut-dependent factor $[(p_W^2 - M_W^2)^2 + \Gamma_W^2 M_W^2]^{-1} [(p_Z^2 - M_Z^2)^2 + \Gamma_Z^2 M_Z^2]^{-1}$, which reproduces the resonant peaking structure.

Of course, a cut on the invariant mass of the $l\nu$ pair is not physical since the longitudinal momentum of the neutrino is not directly measurable. We have therefore imposed the same kind of cuts, but using the transverse mass $M_{\mathrm{T}}(l\nu) = \sqrt{E_{\mathrm{T}}^2(l\nu) - P_{\mathrm{T}}^2(l\nu)}$ as physical quantity instead of the $M(l\nu)$ invariant mass and releasing the lower cut on $M_{\mathrm{T}}(l\nu)$.

The conclusion is similar. The DR contribution differs at the order of ten per cent from the previous case, as shown by the dotted curve in Fig. 5. The full calculation, which represents the true observable, and the DPA are instead rather insensitive to this change.

In the following, we assume the additional kinematical cuts

$$M_{\mathrm{T}}(l\nu) < M_{\mathrm{W}} + 20\,\mathrm{GeV}, \qquad |M(l'\bar{l}') - M_{\mathrm{Z}}| < 20\,\mathrm{GeV} \qquad (4.1)$$

under which exact result and DPA coincide at per-cent level, with a modest loss of signal, as shown in Fig. 4 where the lower solid line represents the full result after imposing the above-mentioned cuts. Since the exact cross section for the process $pp \to 4f$ is rather well approximated by the DPA if proper cuts are applied, we can safely adopt the DPA for computing electroweak radiative corrections. Let us notice, however, that electroweak radiative contributions are not much larger than 20% in the region of experimental sensitivity, as shown in the next section, and the DPA differs from the exact result by less than 15%. Therefore, without imposing the additional cuts (4.1), the error induced by use of the DPA in computing $\mathcal{O}(\alpha)$ contributions would give rise to an uncertainty of less than 3% on the total cross section, so well below the statistical accuracy.

4.2   Effects of $\mathcal{O}(\alpha)$ corrections

In this subsection, we discuss the effect of leading-logarithmic electroweak virtual corrections to WZ production in DPA. First of all, one can see in Fig. 3, where the distributions in the reconstructed invariants $\sqrt{\hat{s}}$ and $\sqrt{|\hat{r}|}$ are plotted, that the previously discussed conditions, under which the logarithmic high-energy approximation is valid, are well fulfilled for WZ production at high transverse momentum $P_{\mathrm{T}}(l\bar{l})$. Both the hard-scattering invariant mass $\sqrt{\hat{s}}$ and $\sqrt{|\hat{r}|} = \sqrt{|x_i P_i - p(l\bar{l})|^2}$, where $x_i P_i$ is the momentum of the parton from one of the protons ($\hat{r}$ corresponds to $\hat{t}$ or $\hat{u}$ depending on the partonic process), are in fact much larger than the boson masses. We have checked in addition that most part of the contribution to the cross section comes from the region where the scattering angle of the reconstructed Z boson in the WZ rest-frame is in the central range with respect to the beam. Finally, as to the ratios between the different invariants which appear in the logarithms, we have verified that the pure angular-dependent ones are mostly in the range $1 < \hat{s}/|\hat{r}| < 6$, while $\hat{s}/M_{\mathrm{W}}^2 > 50$ thus allowing to omit $\log^2(|\hat{r}|/\hat{s})$ type of logarithms up to an accuracy of a few per cent.

As already mentioned in Sect. 3, we perform the computation of radiative corrections to the full process $pp \to 4f$ in DPA, using the complete expressions given in App. A, i.e. implementing the full (SU(2)-transformed) Born matrix elements as in (A.12), (A.13), (A.18), and (A.21)–(A.23). We have verified that the results obtained by making use of the high-energy approximation for the Born amplitudes given in (A.7) and (A.8) are in very good agreement. For all results given in the following, the difference between the two methods is in fact at per-mille level. This comparison shows the reliability of the high-energy approximation for the Born matrix elements, under which the correction factor can be factorized and expressed in a very compact and simple form, leading to considerable decrease of CPU time.

In order to discuss the basic structure of radiative corrections, we first consider the $\mathcal{O}(\alpha)$ contributions to the partonic subprocess $\bar{d}u \to W^+Z$. In Fig. 6a we plot the
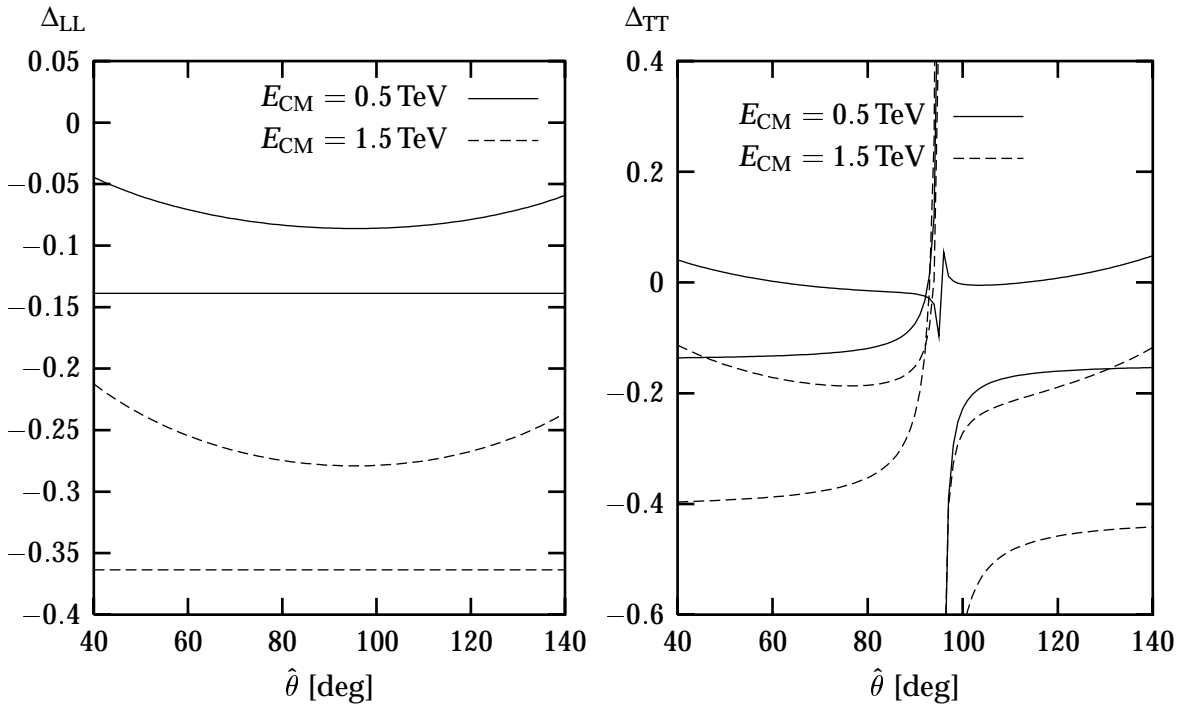
12

Figure 6: (a) Relative corrections Δ_{LL} to the angular distributions for the process $\bar{d}u \to W_L^+ Z_L$. For each CM energy, the upper curves include the complete logarithmic corrections, the lower curves only the angular-independent logarithms. (b) The same for the process $\bar{d}u \to W_T^+ Z_T$.

relative correction to the angular distribution of the longitudinal component $\Delta_{LL} = (d\sigma^{LL}/d\cos\hat{\theta} - d\sigma^{LL}_{Born}/d\cos\hat{\theta})/(d\sigma^{LL}_{Born}/d\cos\hat{\theta})$ with $\sigma = \sigma(\bar{d}u \to W^+ Z)$ as a function of the angle $\hat{\theta}$ between the Z boson and the $\bar{d}$ quark in the $\bar{d}u$ CM frame for the two energies $E_{CM} = 0.5\,\text{TeV}$ and $1.5\,\text{TeV}$. As can be seen, the LL part receives sizeable corrections, in particular in the central region $\hat{\theta} \simeq 90°$ where σ_{LL} is more enhanced. In order to pinpoint the effect of the angular-dependent contributions to the radiative corrections, in the same figure we have also plotted the two flat curves which include only angular-independent logarithms of $\hat{s}/M_W^2$. The difference between the two results for each CM energy shows the importance of taking into account leading and full subleading terms. There are in fact partial cancellations occurring between angular-dependent and angular-independent parts, which sizeably lower the overall corrections (see also Ref. [24]).

For the transverse part σ_{TT} the corresponding relative corrections Δ_{TT} are shown in Fig. 6b for two values of E_{CM} as in the previous figure. Here, radiative-correction effects are less pronounced compared to the LL case, especially at extreme angles where σ_{TT} receives its maximal contribution. The spikes in Fig. 6b originate from the radiation zero of the lowest-order cross section (see Fig. 1), the absolute corrections behave smoothly everywhere. The angular behaviour of Δ_{TT} is more complex, compared with the longitudinal one. The dependence on the angle has in fact a two-fold origin. In addition to the angular-dependent logarithms [see (A.18) and (A.19)], there are angular-independent dou-
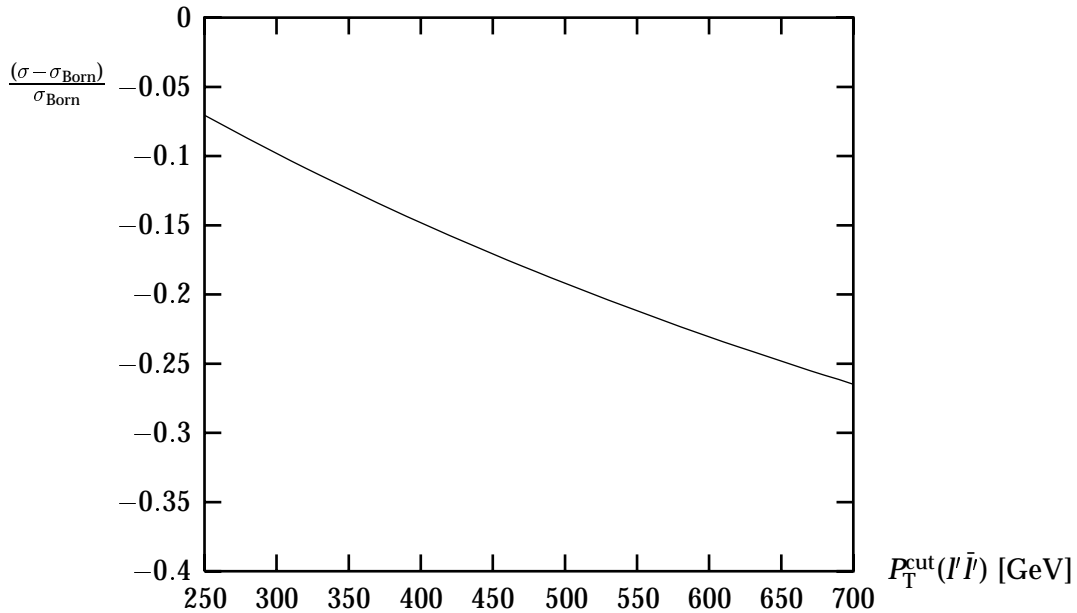
Figure 7: Relative correction to the total cross section for the full process pp $\to l\nu_l l'\bar{l'}$ at $\sqrt{s} = 14\,\mathrm{TeV}$ as a function of the cut on the reconstructed Z-boson transverse momentum. Standard cuts are applied.

ble logarithms $\log^2(\hat{s}/M_W^2)$ with angular-dependent coefficients [see (A.13) and (A.15)], which originate from the mixing of the final Z boson with the photon, induced by virtual soft–collinear W bosons. In Fig. 6b we have reported the total deviation Δ_{TT}, represented for each CM energy by the upper curves, and the partial contribution coming from the angular-independent logarithms of $\hat{s}/M_W^2$, given by the lower lines. As can be seen, also in this case, the correction factors proportional to the angular-dependent and angular-independent logarithms have opposite sign, leading as before to a reduction of the total correction.

In order to show the effect of the electroweak radiative corrections on the complete process pp $\to 4f$, in Fig. 7 we have plotted the $\mathcal{O}(\alpha)$ correction relative to the total Born cross section, $\Delta = (\sigma - \sigma_{\mathrm{Born}})/\sigma_{\mathrm{Born}}$, as a function of the cut on the transverse momentum of the reconstructed Z boson, $P_{\mathrm{T}}^{\mathrm{cut}}(l\bar{l})$. Our standard cuts are applied. As can be seen, the $\mathcal{O}(\alpha)$ contributions are negative and get larger with increasing $P_{\mathrm{T}}^{\mathrm{cut}}$, roughly going from -5% to -25% in the considered momentum range. The relatively large size of the radiative corrections, especially at energies which are at first sight rather modest (e.g. $P_{\mathrm{T}}^{\mathrm{cut}} > 250\,\mathrm{GeV}$ implies $\sqrt{\hat{s}} > 500\,\mathrm{GeV}$), is mainly due to two combined effects. On one side, the longitudinal component of the cross section, σ_{LL}, which dominates at low values of the allowed energy range, as shown in Fig. 2 (right side), where the scattering angles are dominantly central, generates sizeable corrections. On the other hand, as can be seen in Fig. 3, the total cross section even for modest values of $P_{\mathrm{T}}^{\mathrm{cut}}$ receives a substantial contribution from the very-high-energy region, where σ_{TT} dominates. So, the generally smaller $\mathcal{O}(\alpha)$ contributions from the TT configuration, as compared with the LL ones, get enhanced by the higher values of the CM energy, and give globally additional sizeable
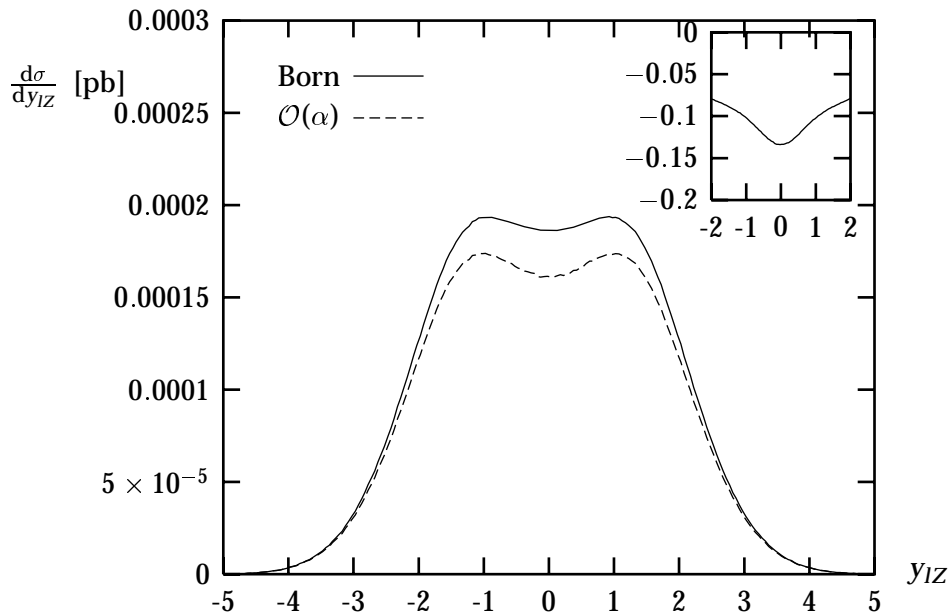
14

Figure 8: Rapidity distribution for the full process $pp \to l\nu_l l'\bar{l}'$ at $\sqrt{s} = 14\,\mathrm{TeV}$. Standard cuts and $P_\mathrm{T}(l'\bar{l}') > 300\,\mathrm{GeV}$ are applied. The inset plot shows the difference between $\mathcal{O}(\alpha)$ and Born results normalized to the Born distribution.

effects. As a consequence, the corrections to the total cross section are large because the P_T cut selects high-energy domains (since the only way to obtain a large $P_\mathrm{T}(l\bar{l})$ is to have a large WZ invariant mass) and enhances the contributions coming from the central angular region. This shows that the size of the radiative contributions is strictly dependent on the applied cuts and the selected kinematical configurations.

This is even more clearly visible in Fig. 8, where we have plotted the distribution in the difference between the rapidity of the reconstructed Z boson and of the charged lepton coming from the decay of the W, $\Delta y_{\mathrm{Z}l} = y(l'\bar{l}') - y(l)$, at Born level (solid line) and including radiative corrections (dashed line). The rapidity is defined from the energy E and the longitudinal momentum P_L by $y = 0.5 \log((E + P_\mathrm{L})/(E - P_\mathrm{L}))$. This variable, studied in Ref. [4] and defined in terms of direct observables, is symmetric around zero and shows a residual dip reflecting the approximate radiation zero of the angular distribution of the Born WZ production. The quantity $\Delta y_{\mathrm{Z}l}$ is in fact similar to the rapidity difference $\Delta y_{\mathrm{ZW}} = y_\mathrm{W} - y_\mathrm{Z}$ considered in Ref. [8], which is strictly related to the scattering angle, $\hat{\theta}$, of the Z boson in the WZ rest-frame. The definition of Δy_{ZW} and $\cos \hat{\theta}$ requires, however, the reconstruction of the unknown longitudinal momentum of the neutrino. Even if this can be derived by assuming the W boson to be on-shell [25], the two-fold ambiguity given by the two possible solutions for the neutrino longitudinal momentum spoils the radiation zero. Therefore, in order to extract informations about the angular dependence of the WZ process, it is preferable to use $\Delta y_{\mathrm{Z}l}$ [26].

The first information one can get from Fig. 8 is that the main contribution to the cross section originates from small values of $\Delta y_{\mathrm{Z}l}$ corresponding to central scattering angles. At the LHC, for the first time the statistics will be sufficient to experimentally

$pp \rightarrow l\nu_l l'\bar{l'}$				
$P_{\mathrm{T}}^{\mathrm{cut}}(l'\bar{l'})$ [GeV]	σ_{Born} [fb]	σ [fb]	Δ [%]	$1/\sqrt{2L\sigma_{\mathrm{Born}}}$ [%]
250	1.716	1.595	-7.1	5.4
300	0.899	0.811	-9.8	7.5
350	0.503	0.441	-12.4	10
400	0.296	0.252	-14.9	13
450	0.181	0.150	-17.1	16.6
500	0.114	0.092	-19.3	20.9

Table 1: Cross section for $pp \rightarrow l\nu_l l'\bar{l'}$ for various values of $P_{\mathrm{T}}^{\mathrm{cut}}(l'\bar{l'})$

test the behaviour due to the approximate radiation zero, which might be distorted by new-physics contributions. Figure 8 indicates that radiative effects are maximal at small rapidity separation, which is the region of stronger sensitivity to new physics. Moreover, owing to the applied cuts, these relatively large radiative contributions are not due to the suppression of the tree-level cross section and, being negative, they even slightly enhance the residual dip.

The above-discussed effects should of course be compared with the expected experimental accuracy. In Table 1 we have listed the relative deviation Δ and the statistical error, estimated by assuming a luminosity $L = 100\,\mathrm{fb}^{-1}$ for two experiments, for some $P_{\mathrm{T}}^{\mathrm{cut}}$ values. This comparison indicates that at high transverse momentum of the gauge bosons the virtual electroweak corrections are non-negligible and can be comparable with the experimental accuracy up to about $500\,\mathrm{GeV}$. In this region the corrections range between -5 and -20%. Whether or not they should be taken into account when performing analyses in this kinematical region depends of course on the available luminosity. Only in a high-luminosity run their effect will be relevant.

5 $W^{\pm}\gamma$ production

In this section, we extend our analysis to the process $pp \rightarrow l\nu_l\gamma$ ($l = \mathrm{e}, \mu$). This channel, proper for the measurement of the trilinear gauge-boson coupling $WW\gamma$, can furnish complementary informations on the vertex structure of the SM when combined with the analysis of WZ production. As before, we consider the region of high CM energies of the hard scattering, where the sensitivity to new-physics effects is expected to be more enhanced, and the precise knowledge of the SM background can be then particularly useful. In the following we analyse the same set of variables used to discuss the WZ production process and the effect of the $\mathcal{O}(\alpha)$ electroweak corrections on them.
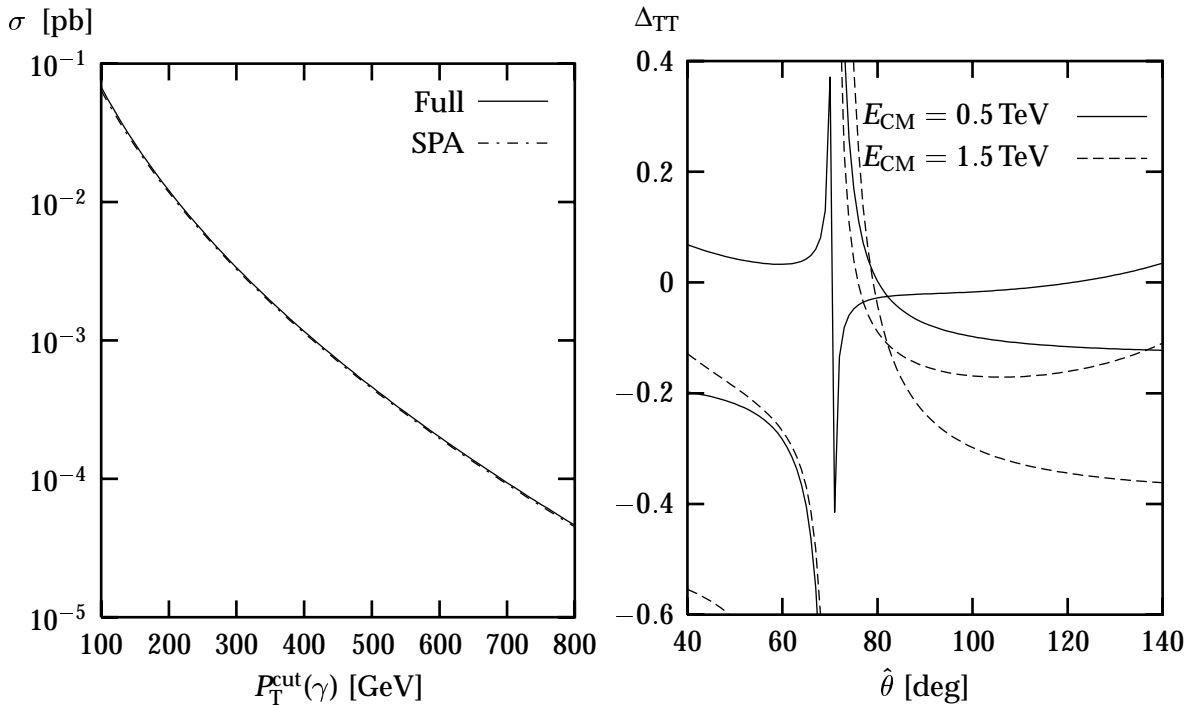
Figure 9: (a) Born cross section for the full process pp $\to l\nu_l\gamma$ at $\sqrt{s} = 14\,\text{TeV}$ as a function of the cut on the photon transverse momentum. Standard cuts are applied. (b) Relative corrections to the angular distribution for the subprocess $\bar{\text{d}}\text{u} \to W_T^+\gamma$. The two upper and lower curves for each energy are as in Fig. 6b.

5.1 Born level

The partonic subprocess $\bar{\text{d}}\text{u} \to W^+\gamma$ is dominated by the production of two transverse gauge bosons, whereas the remaining (LT) helicity configuration is suppressed by a factor M_W/E_{CM} in the high-energy limit. All features discussed in Sect. 4.1 for the subprocess $\bar{\text{d}}\text{u} \to W_T^+Z_T$ with transversely polarized gauge bosons qualitatively apply as well to $W\gamma$ production. The corresponding cross section is in fact strongly peaked in the forward and backward directions and presents a radiation zero for $\cos\hat{\theta} = (Q_u + Q_d)/(Q_u - Q_d) = 1/3$ where $\hat{\theta}$ is the angle between the $\bar{\text{d}}$ quark and the photon. As to the general behaviour of the $\bar{\text{d}}\text{u} \to W^+\gamma$ process, we refer back to Figs. 1 and 2 and details given in the text.

In spite of these similarities, $W\gamma$ production presents, however, some different characteristics with respect to the WZ case. First of all, owing to the absence of any pure non-suppressed longitudinal components, there are no sizeable gauge cancellations in the total cross section of the full process pp $\to l\nu_l\gamma$ at high energy. The resonant contribution (pp $\to W\gamma \to l\nu_l\gamma$) is always lower than the full result, also for high values of the cut on the photon transverse momentum $P_T(\gamma)$, and the difference between the two cross sections is below 3%. Therefore, one can still consider the pure resonant part as a useful definition of the $W\gamma$ signal. Also, the single-pole approximation (SPA) defined in (3.2) differs negligibly from the exact result, as shown in Fig. 9a, where we have plotted the total cross section versus the cut applied on the photon transverse momentum. One

17

could directly use the SPA to compute radiative corrections at the per-cent level without imposing any additional cuts. However, for sake of uniformity, in the following we apply the same kind of cut $M_{\mathrm{T}}(l\nu) < M_{\mathrm{W}} + 20\,\mathrm{GeV}$ as used for the WZ process, under which resonant, full, and SPA cross sections converge to the same value within one per cent and with a negligible loss of signal.

5.2   Effect of $\mathcal{O}(\alpha)$ corrections

In this subsection, we study the effect of virtual electroweak radiative corrections on $\mathrm{W}\gamma$ production in SPA. We consider first the partonic subprocess $\bar{\mathrm{d}}\mathrm{u} \to \mathrm{W}^+\gamma$. In Fig. 9b we have plotted $\Delta_{\mathrm{TT}} = (\mathrm{d}\sigma^{\mathrm{TT}}/\mathrm{d}\cos\hat{\theta} - \mathrm{d}\sigma^{\mathrm{TT}}_{\mathrm{Born}}/\mathrm{d}\cos\hat{\theta})/(\mathrm{d}\sigma^{\mathrm{TT}}_{\mathrm{Born}}/\mathrm{d}\cos\hat{\theta})$ as a function of the angle $\hat{\theta}$ between the $\bar{\mathrm{d}}$ quark and the photon. As can be seen, the behaviour of the $\mathcal{O}(\alpha)$ contributions is quite similar to the $\mathrm{W_T Z_T}$ case. Only the spikes, again due to the radiation zero, are correspondingly shifted, and reverse the shape of the curves with respect to the angle, compared with Fig. 6b.

As in the previous case, the validity conditions of the high-energy logarithmic approximation for the radiative corrections are well satisfied by the complete process $\mathrm{pp} \to l\nu_l\gamma$. The kinematical behaviour of $\mathrm{W}\gamma$ at high transverse momentum of the photon reproduces in fact the same shape of the distributions as in Fig. 3. All invariants are then much larger than the boson masses, and at fixed $P_{\mathrm{T}}^{\mathrm{cut}}(\gamma)$ the process receives considerable contributions from very high CM energies. We have moreover verified that, despite the radiation zero and the absence of any non-mass-suppressed longitudinal components, for large $P_{\mathrm{T}}^{\mathrm{cut}}(\gamma)$ values ($P_{\mathrm{T}}^{\mathrm{cut}}(\gamma) \gtrsim 250\,\mathrm{GeV}$) most part of the contribution to the total cross section comes from the region of phase space where the photon is emitted at large angle with respect to the beam (see also Fig. 11).

In order to show the effect of radiative corrections on the full process $\mathrm{pp} \to l\nu_l\gamma$, we have plotted as before the $\mathcal{O}(\alpha)$ corrections relative to the Born cross section as a function of the cut on the transverse momentum of the photon in Fig. 10. The overall behaviour is quite similar to the WZ case; the size of the radiative effects is, however, lower.

This affects in the same way also the distribution in the difference between the rapidity of the photon and the charged lepton coming from W-boson decay [26], $\Delta y_{l\gamma} = y_l - y_\gamma$, plotted in Fig. 11. Here, unlike in the previous case, the dip reflecting the radiation zero is much more pronounced, but the radiative corrections slightly decrease going towards $\Delta y_{l\gamma} = 0$. Owing to the different location of the radiation zero, the radiative contribution for very small rapidity separation is still sizeable, but it does not get enhanced as for the WZ process, where in the same region the longitudinal component gives the dominant contribution. Hence for $\mathrm{W}\gamma$, despite the complex behaviour shown in Fig. 9b, which is merely due to the fictitious spikes, the radiative-correction effect is rather uniform in the angular range we consider, and leads to an overall rescaling of the $\Delta y_{l\gamma}$ distribution by roughly a factor 0.9. These effects could still mimic the behaviour of new-physics contributions. Their smaller size, compared with the WZ case, is compensated by the larger value of the overall cross section. Therefore, even if not extremely enhanced in the central rapidity range, radiative effects can become comparable with the statistical error.

In Tab. 2 we compare the $\mathcal{O}(\alpha)$ relative correction Δ to the Born cross section with the expected experimental accuracy, assuming $L = 100\,\mathrm{fb}^{-1}$ for two experiments, for different
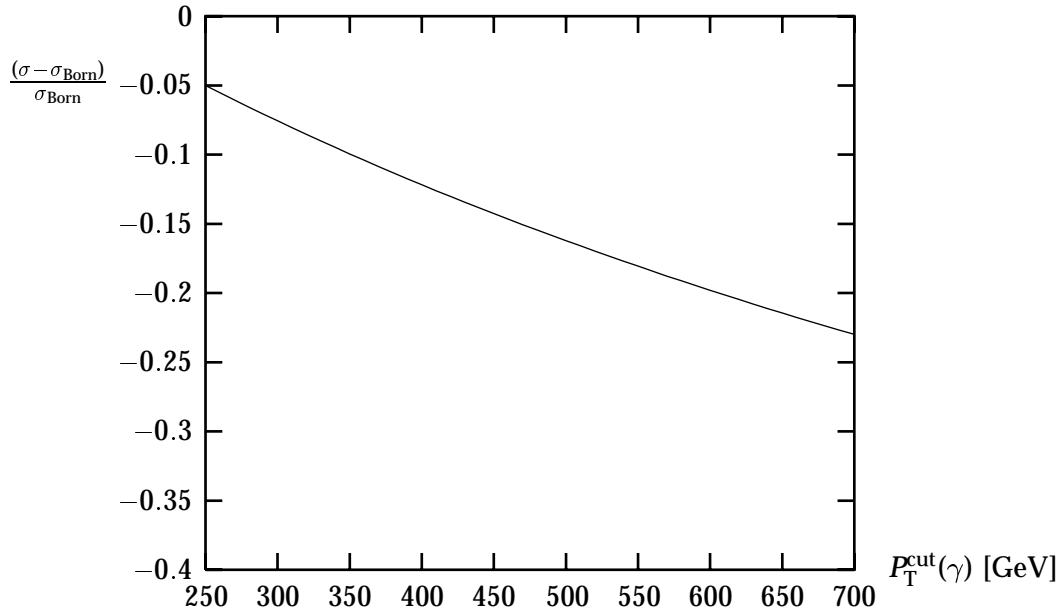
Figure 10: Relative corrections to the cross section for the full process pp $\rightarrow l\nu_l\gamma$ at $\sqrt{s} = 14\,\text{TeV}$ as a function of the cut on the photon transverse momentum. Standard cuts are applied.
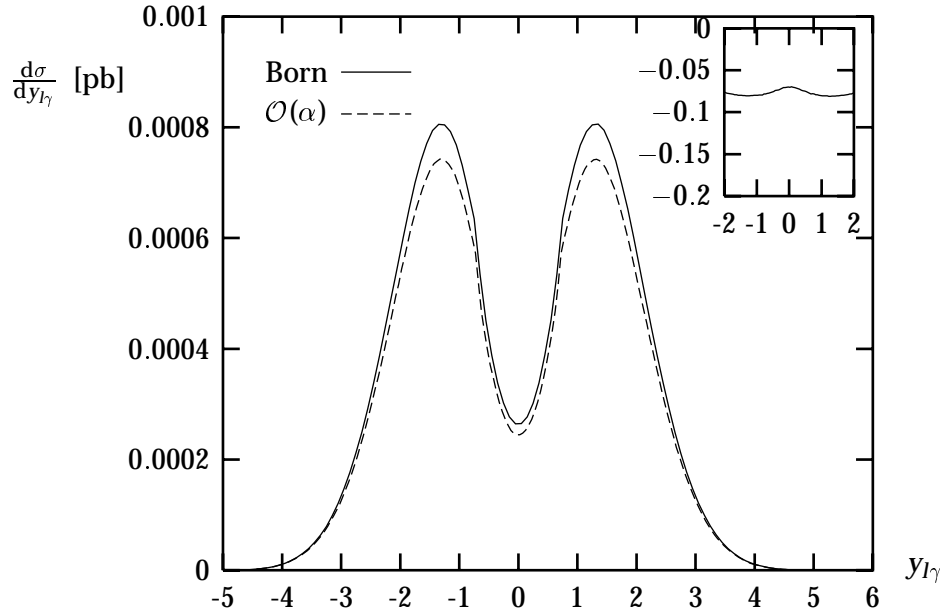

Figure 11: Rapidity distribution for the full process pp $\rightarrow l\nu_l\gamma$ at $\sqrt{s} = 14\,\text{TeV}$. Standard cuts and $P_\text{T}(\gamma) > 300\,\text{GeV}$ are applied. The inset plot shows the difference between $\mathcal{O}(\alpha)$ and Born results normalized to the Born distribution.

values of $P_\mathrm{T}^\mathrm{cut}(\gamma)$. As one can see, radiative effects are very sensitive to $P_\mathrm{T}^\mathrm{cut}(\gamma)$ and, despite

	pp $\to l\nu_l\gamma$			
$P_\mathrm{T}^\mathrm{cut}(\gamma)$ [GeV]	σ_Born [fb]	σ [fb]	Δ [%]	$1/\sqrt{2L\sigma_\mathrm{Born}}$ [%]
250	5.810	5.519	-5.0	2.9
300	3.180	2.940	-7.6	4.0
350	1.832	1.650	-10.0	5.2
400	1.100	0.966	-12.2	6.7
450	0.684	0.587	-14.2	8.6
500	0.437	0.366	-16.2	10.7
550	0.285	0.234	-18.0	13.2
600	0.190	0.152	-19.8	16.2
650	0.129	0.101	-21.4	19.6
700	0.089	0.068	-23.3	23.7

Table 2: Cross section for pp $\to l\nu_l\gamma$ for various values of $P_\mathrm{T}^\mathrm{cut}(\gamma)$.

of the decrease of the cross section with increasing $P_\mathrm{T}^\mathrm{cut}(\gamma)$, are larger than the statistical error for $P_\mathrm{T}^\mathrm{cut}(\gamma)$ below $700\,\mathrm{GeV}$, where they range from -5 to -23%. Moreover, they could be of some relevance also in a low-luminosity run ($L = 30\,\mathrm{fb}^{-1}$) of the LHC, as they might become comparable with the experimental precision for $P_\mathrm{T}^\mathrm{cut}(\gamma) < 400\,\mathrm{GeV}$.

6   Conclusion

By means of a complete four-fermion calculation, we have examined WZ production in the purely leptonic channel at the LHC. An analogous computation has been performed for the Wγ process followed by the leptonic W decay. We have given some examples of phenomenological analyses relevant to hadronic di-boson production in the high di-boson invariant-mass region.

At tree level, we have found that, for processes involving WZ production, the diagrammatic approach usually adopted to isolate the signal is not viable anymore at large transverse momentum of the reconstructed Z boson, owing to gauge cancellations. The doubly-resonant approximation can differ from the full result by tens of per cent in experimentally relevant regions. The only sensible observable is the total contribution. Moreover the two commonly used approximations, narrow-width (i.e. *production × decay*) and leading pole approximation, can underestimate the exact result by about 10–15% at relatively modest energies, if no cuts are applied.

The primary aim of our analysis was to investigate the structure of virtual electroweak corrections and their effect on di-boson production processes at the LHC. The one-loop leading-logarithmic corrections to the full four-fermion or two-fermion-plus-photon process have been calculated in leading-pole approximation, neglecting non-factorizable corrections, and restricting oneself to the gauge-invariant leading-logarithmic corrections, which only contribute to the gauge-boson pair-production subprocess. We found that this approach constitutes a reliable approximation in the high-P_T region at the LHC.

In order to illustrate the behaviour and the size of $\mathcal{O}(\alpha)$ contributions, we have presented different cross sections and distributions. In this study, we have not included the full QED radiative contributions, which involve also the emission of real photons and therefore depend on the detector resolution. We focused instead on the contributions of the leading electroweak logarithms resulting from above the electroweak scale.

For WZ and Wγ production processes, electroweak corrections turn out to be non-negligible in the high-energy region of the hard process, in particular for large transverse momentum and small rapidity separation of the reconstructed vector bosons, which is the kinematical range of maximal sensitivity to new-physics phenomena. Electroweak radiative effects lower the Born results by 5–20% in the region of experimental sensitivity. We have moreover shown that their size depends sensibly not only on the CM energy but also on the applied cuts and varies according to the selected observables and kinematical regions. Despite of the strong decrease of the cross section with increasing di-boson invariant mass, radiative effects can still be appreciable if compared with the expected experimental precision. This depends of course on the available luminosity. For WZ production, these effects are relevant for the high-luminosity run of the LHC. Owing to their larger overall cross section, Wγ production processes can instead show a sensitivity to radiative effects also at low luminosity.

Acknowledgements

A   Logarithmic electroweak corrections

In this section, we present the analytical formulas for the logarithmic electroweak corrections to the polarized partonic subprocesses

$$\bar{\mathrm{d}}_\mathrm{L}(p_{\bar{\mathrm{d}}})\,\mathrm{u}_\mathrm{L}(p_\mathrm{u}) \to \mathrm{W}^+_{\lambda_\mathrm{W}}(p_\mathrm{W})\,N_{\lambda_N}(p_N), \qquad N = A, \mathrm{Z}, \tag{A.1}$$

which can be derived from the general results given in Ref. [13]. The label L indicates the left-handed chirality of the initial-state quarks (right-handed quarks are not considered since they cannot produce W bosons), and $\lambda_{\mathrm{W},N} = 0, \pm 1$ represent the gauge-boson helicities. The photon field is denoted by A in this appendix. The Mandelstam variables read $\hat{s} = (p_{\bar{\mathrm{d}}} + p_\mathrm{u})^2$, $\hat{t} = (p_{\bar{\mathrm{d}}} - p_{\mathrm{W}^+})^2$, and $\hat{u} = (p_{\bar{\mathrm{d}}} - p_N)^2$, where the momenta of the initial and final states are incoming and outgoing, respectively. In the high-energy limit,

we have $\hat{t} \sim -\hat{s}(1 + \cos\hat{\theta})/2$ and $\hat{u} \sim -\hat{s}(1 - \cos\hat{\theta})/2$, where $\hat{\theta}$ is the angle between $\vec{p}_{\bar{d}}$ and $\vec{p}_N$, in the CM frame of the scattering quarks.

For the calculation of the cross section (2.2) we need besides the process $\bar{d}u \rightarrow W^+N$ also its charge conjugate and the cross sections for exchanged initial quarks. These latter can be obtained from one another just by exchanging the invariants $\hat{t} \leftrightarrow \hat{u}$. Owing to CP invariance, the charge-conjugate processes can be instead obtained from the initial processes by applying a parity transformation,

$$\mathcal{M}\left[d(p_d)\bar{u}(p_{\bar{u}}) \rightarrow W^-(p_W)N(p_N)\right] = \mathcal{M}\left[\bar{d}(\tilde{p}_{\bar{d}})u(\tilde{p}_{\bar{u}}) \rightarrow W^+(\tilde{p}_W)N(\tilde{p}_N)\right] \qquad (A.2)$$

with $\tilde{p} = (E, -\vec{p})$ for $p = (E, \vec{p})$. So, also in this case, the correction factors can be obtained from the same initial process (A.1). The formulas we give in the following for the process (A.1) can therefore cover all contributions we need for the complete WZ and $W\gamma$ production processes.

The one-loop corrections are evaluated in the limit

$$\hat{s} \sim \hat{t} \sim \hat{u} \gg M_W^2, \qquad (A.3)$$

and we restrict ourselves to the combinations of gauge-boson helicities that are not mass-suppressed compared with $\sqrt{\hat{s}}$ in this limit. These correspond to the purely transverse and opposite final state $(\lambda_W, \lambda_N) = (\pm, \mp)$, which we denote by $(\lambda_W, \lambda_N) = (T, T)$, and, in the case of $W^\pm Z$ production, also to the purely longitudinal final state $(\lambda_W, \lambda_Z) = (0, 0)$, which we denote by $(\lambda_W, \lambda_Z) = (L, L)$.

A.1 One-loop corrections

In the following, we present the results as relative corrections

$$\delta_{\bar{d}_L u_L \rightarrow W_\lambda^+ N_\lambda} = \frac{\delta\mathcal{M}_{\text{virt}}^{\bar{d}_L u_L \rightarrow W_\lambda^+ N_\lambda}(p_{\bar{d}}, p_u, p_W, p_N)}{\mathcal{M}_{\text{Born}}^{\bar{d}_L u_L \rightarrow W_\lambda^+ N_\lambda}(p_{\bar{d}}, p_u, p_W, p_N)} \qquad (A.4)$$

to the Born matrix elements. A more detailed derivation can be found in Ref. [27].

As shown in Ref. [13], in the high-energy logarithmic approximation the longitudinal gauge bosons can be replaced by the corresponding would-be Goldstone bosons. Therefore, in our results for longitudinal final states $(\lambda = L)$, the substitutions $W_L^\pm \rightarrow \phi^\pm$ and $Z_L \rightarrow \chi$ have to be performed.

The corrections (A.4) are split as

$$\delta = \delta^{\text{LSC}} + \delta^{\text{SSC}} + \delta^{\text{C}} + \delta^{\text{PR}} \qquad (A.5)$$

into leading (δ^{LSC}) and subleading (δ^{SSC}) contributions originating from soft–collinear gauge bosons, contributions δ^{C} that originate from collinear (or soft) gauge bosons and from wave-function renormalization, and contributions δ^{PR} that originate from parameter renormalization. All these corrections are evaluated in logarithmic approximation, i.e. including all terms that involve logarithms of the form $\log(\hat{s}/M_W^2)$ in the high-energy limit. More precisely, we restrict ourselves to
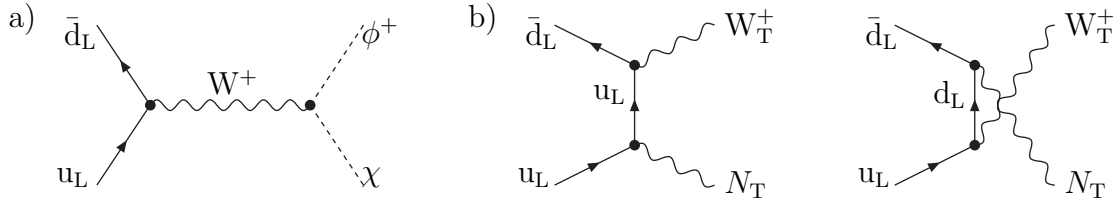
Figure 12: Dominant lowest-order diagrams for $\bar{d}_L u_L \to \phi^+ \chi$ and $\bar{d}_L u_L \to W_T^+ N_T$

- the angular-independent double- and single-logarithmic corrections of the type $\alpha \log^2 (\hat{s}/M_W^2)$ and $\alpha \log (\hat{s}/M_W^2)$, which involve only the ratio of the CM energy to the W-boson mass,

- the double logarithms of the form $\alpha \log (\hat{s}/M_W^2) \log(M_Z^2/M_W^2)$, and

- the angular-dependent double logarithms of the type $\alpha \log (\hat{s}/M_W^2) \log (|\hat{r}|/\hat{s})$, with $\hat{r} = \hat{t}, \hat{u}$.

For completeness we give also the analytic expressions of the double- and single-logarithmic corrections that contain logarithms $\log (M_W^2/\lambda^2)$ and $\log(M_W^2/m_f^2)$, which involve the photon mass λ or masses of light charged fermions.[1] These contributions, denoted by L^{em} and l^{em} in the following, are of pure electromagnetic origin and are not included into the numerical studies.

The coefficients of the various logarithmic terms are expressed in terms of the eigenvalues $I_\varphi^{V^a}$, or of the matrix components $I_{\varphi\varphi'}^{V^a}$, of the generators[2]

$$I^A = -Q = -\frac{Y}{2} - T^3, \qquad I^Z = -\frac{s_w}{2c_w}Y + \frac{c_w}{s_w}T^3, \qquad I^\pm = \frac{T^1 \pm iT^2}{\sqrt{2}s_w}, \qquad (A.6)$$

where $c_w^2 = 1 - s_w^2 = M_W^2/M_Z^2$.

A.2 Born matrix elements in the high-energy limit

As input for the evaluation of the relative corrections (A.4) we need the Born matrix elements for the processes (A.1) and the SU(2)-transformed Born amplitudes that we list in the following, restricting ourselves to the non-suppressed helicities. The corresponding amplitudes, are given in (A.7) and (A.8) in high-energy approximation, i.e. omitting mass-suppressed terms. As we will see, this leads to very compact analytical expressions for the relative corrections (A.4). However, we recall that in the numerics instead of the high-energy approximations (A.7) and (A.8) the corresponding exact expressions have been used. As noted in Sect. 4.2, the difference is at the per-mille level.

---

[1]This kind of contributions includes also energy-dependent double logarithms of the type $\alpha \log (\hat{s}/M_W^2) \log (M_W^2/\lambda^2)$.

[2]A detailed list of the gauge-group generators and of related quantities that are used in the following can be found in App. B of Ref. [13].

For longitudinally polarized gauge bosons, we consider the Born matrix elements involving the corresponding would-be Goldstone bosons. These are dominated by the s-channel exchange of gauge bosons (see Fig. 12a), and read

$$\mathcal{M}_{\text{Born}}^{\bar{d}_L u_L \to \phi^+ \chi} = \frac{-ie^2}{2\sqrt{2}s_W^2}\frac{A_s}{\hat{s}}, \qquad \mathcal{M}_{\text{Born}}^{\bar{q}_L q_L \to H\chi} = e^2 I_{q_L}^Z I_{\chi H}^Z \frac{A_s}{\hat{s}}, \qquad \mathcal{M}_{\text{Born}}^{\bar{q}_L q_L \to \chi\chi} = 0,$$

$$\mathcal{M}_{\text{Born}}^{\bar{q}_L q_L \to \phi^+ \phi^-} = -e^2 \left(\frac{T_{q_L}^3}{2s_W^2} + \frac{Y_{q_L}}{4c_W^2}\right)\frac{A_s}{\hat{s}}, \qquad q_L = u_L, d_L. \tag{A.7}$$

The production of transverse gauge bosons is dominated by the t- and u-channel contributions (see Fig. 12b) and gives

$$\mathcal{M}_{\text{Born}}^{\bar{d}_L u_L \to W_T^+ N_T} = \frac{e^2}{\sqrt{2}s_W}\left(I_{u_L}^N \frac{1}{\hat{t}} + I_{d_L}^N \frac{1}{\hat{u}}\right)A_t,$$

$$\mathcal{M}_{\text{Born}}^{\bar{q}_L q_L \to N_T' N_T} = e^2 I_{q_L}^{N'} I_{q_L}^N \left(\frac{1}{\hat{t}} + \frac{1}{\hat{u}}\right)A_t, \qquad \mathcal{M}_{\text{Born}}^{\bar{q}_L q_L \to W_T^+ W_T^-} = \frac{e^2}{2s_W^2}\frac{A_t}{\hat{r}}, \tag{A.8}$$

where $\hat{r} = \hat{t}, \hat{u}$ for $q = d, u$, respectively. In order to determine the relative corrections, the explicit dependence of the amplitudes A_s and A_t, in (A.7) and (A.8), on the kinematics and on the helicities need not to be specified.

A.3 Leading soft–collinear corrections

The angular-independent leading soft–collinear (LSC) corrections, which are given in Eqs. (3.6) and (3.7) of Ref. [13], depend on the eigenvalues

$$C_\Phi^{\text{ew}} = \frac{1+2c_W^2}{4s_W^2 c_W^2}, \qquad C_{u_L}^{\text{ew}} = C_{d_L}^{\text{ew}} = C_{q_L}^{\text{ew}} = \frac{s_W^2 + 27c_W^2}{36s_W^2 c_W^2}, \qquad C_W^{\text{ew}} = \frac{2}{s_W^2} \tag{A.9}$$

of the electroweak Casimir operator C^{ew}, on its components

$$C_{AA}^{\text{ew}} = 2, \qquad C_{AZ}^{\text{ew}} = C_{ZA}^{\text{ew}} = -2\frac{c_W}{s_W}, \qquad C_{ZZ}^{\text{ew}} = 2\frac{c_W^2}{s_W^2} \tag{A.10}$$

in the neutral gauge-boson sector, as well as on the squared Z-boson couplings

$$(I_{d_L}^Z)^2 = \frac{(3c_W^2 + s_W^2)^2}{36s_W^2 c_W^2}, \qquad (I_{u_L}^Z)^2 = \frac{(3c_W^2 - s_W^2)^2}{36s_W^2 c_W^2},$$

$$(I_{W^-}^Z)^2 = \frac{c_W^2}{s_W^2}, \qquad (I_{\phi^-}^Z)^2 = \frac{(c_W^2 - s_W^2)^2}{4s_W^2 c_W^2}, \qquad (I_\chi^Z)^2 = \frac{1}{4s_W^2 c_W^2}. \tag{A.11}$$

For longitudinal and transverse gauge bosons we have

$$\begin{aligned}
\delta_{\bar{d}_L u_L \to W_L^+ Z_L}^{\text{LSC}} = \frac{\alpha}{4\pi}\Bigg\{ &- \left[C_{q_L}^{\text{ew}} + C_\Phi^{\text{ew}}\right]\log^2\left(\frac{\hat{s}}{M_W^2}\right) \\
&+ \sum_{\varphi=\bar{d}_L,u_L,\phi^-,\chi} (I_\varphi^Z)^2 \log\left(\frac{\hat{s}}{M_W^2}\right)\log\left(\frac{M_Z^2}{M_W^2}\right)\Bigg\} \\
&- \frac{1}{2}\sum_{\varphi=\bar{d}_L,u_L,\phi^-} Q_\varphi^2 L^{\text{em}}(\hat{s},\lambda^2,m_\varphi^2),
\end{aligned} \tag{A.12}$$

24

and

$$\delta^{\text{LSC}}_{\bar{d}_L u_L \to W_T^+ N_T} = \frac{\alpha}{4\pi} \left\{ -\frac{1}{2} \left[\sum_{\varphi=\bar{d}_L,u_L,W^-} C^{\text{ew}}_\varphi + \sum_{N'} C^{\text{ew}}_{N'N} \frac{\mathcal{M}^{\bar{d}_L u_L \to W_T^+ N_T'}_{\text{Born}}}{\mathcal{M}^{\bar{d}_L u_L \to W_T^+ N_T}_{\text{Born}}} \right] \log^2 \left(\frac{\hat{s}}{M_W^2} \right) \right.$$

$$+ \sum_{\varphi=\bar{d}_L,u_L,W^-} (I^Z_\varphi)^2 \log \left(\frac{\hat{s}}{M_W^2} \right) \log \left(\frac{M_Z^2}{M_W^2} \right) \Bigg\}$$

$$- \frac{1}{2} \sum_{\varphi=\bar{d}_L,u_L,W^-} Q_\varphi^2 L^{\text{em}}(\hat{s}, \lambda^2, m_\varphi^2), \tag{A.13}$$

respectively, where the electromagnetic logarithms $L^{\text{em}}(\hat{s}, \lambda^2, M_\varphi^2)$ are given by

$$L^{\text{em}}(\hat{s}, \lambda^2, m_\varphi^2) = \frac{\alpha}{4\pi} \left\{ 2 \log \left(\frac{\hat{s}}{M_W^2} \right) \log \left(\frac{M_W^2}{\lambda^2} \right) + \log^2 \left(\frac{M_W^2}{\lambda^2} \right) - \log^2 \left(\frac{m_\varphi^2}{\lambda^2} \right) \right\}. \tag{A.14}$$

For transverse final states, the non-diagonal components C^{ew}_{AZ} and C^{ew}_{ZA} of the electroweak Casimir operator require the evaluation of the transformed matrix elements with $N' \neq N$. Using the high-energy approximation of the Born matrix elements (A.8), (A.13) can be written as

$$\delta^{\text{LSC}}_{\bar{d}_L u_L \to W_T^+ N_T} = \frac{\alpha}{4\pi} \left\{ - \left[C^{\text{ew}}_{q_L} + \frac{1}{2} C^{\text{ew}}_W \left(1 + G^N_- \right) \right] \log^2 \left(\frac{\hat{s}}{M_W^2} \right) \right.$$

$$+ \sum_{\varphi=\bar{d}_L,u_L,W^-} (I^Z_\varphi)^2 \log \left(\frac{\hat{s}}{M_W^2} \right) \log \left(\frac{M_Z^2}{M_W^2} \right) \Bigg\}$$

$$- \frac{1}{2} \sum_{\varphi=\bar{d}_L,u_L,W^-} Q_\varphi^2 L^{\text{em}}(\hat{s}, \lambda^2, m_\varphi^2), \tag{A.15}$$

with the angular-dependent functions

$$G^A_\pm = \frac{F_\pm}{F_- + Y_{q_L} F_+}, \qquad G^Z_\pm = \frac{c_W^2 F_\pm}{c_W^2 F_- - s_W^2 Y_{q_L} F_+}, \tag{A.16}$$

and

$$F_\pm = \left(\frac{1}{\hat{t}} \pm \frac{1}{\hat{u}} \right). \tag{A.17}$$

A.4   Subleading soft–collinear corrections

The angular-dependent subleading soft–collinear (SSC) corrections are obtained by applying the formula (3.12) of Ref. [13], to the crossing symmetric process $\bar{d}_L(p_{\bar{d}}) \, u_L(p_u) \, W^-_{\lambda_W}(-p_W) \, N_{\lambda_N}(-p_N) \to 0$, with $r_{12} = \hat{s}$, $r_{13} = \hat{t}$, and $r_{14} = \hat{u}$. This yields

$$\delta^{\text{SSC}}_{\bar{d}_L u_L \to W_\lambda^+ N_\lambda} = \frac{\alpha}{4\pi} \sum_{V^a=A,Z} 2 \left[\log \left(\frac{\hat{s}}{M_W^2} \right) + \log \left(\frac{M_W^2}{M_{V^a}^2} \right) \right]$$

$$\times I_{W_\lambda^-}^{V^a} \left[I_{\bar{d}_L}^{V^a} \log\left(\frac{|\hat{t}|}{\hat{s}}\right) + I_{u_L}^{V^a} \log\left(\frac{|\hat{u}|}{\hat{s}}\right) \right]$$

$$+ \frac{\alpha}{4\pi} \left\{ 2\log\left(\frac{\hat{s}}{M_W^2}\right) \sum_{N_\lambda'} I_{N_\lambda' N_\lambda}^Z \mathcal{M}_{\text{Born}}^{\bar{d}_L u_L \to W_\lambda^+ N_\lambda'} \left[I_{\bar{d}_L}^Z \log\left(\frac{|\hat{u}|}{\hat{s}}\right) + I_{u_L}^Z \log\left(\frac{|\hat{t}|}{\hat{s}}\right) \right] \right.$$

$$- \frac{2}{\sqrt{2}s_W} \log\left(\frac{\hat{s}}{M_W^2}\right) \left[\left(\sum_{N_\lambda'} I_{N_\lambda'}^+ \mathcal{M}_{\text{Born}}^{\bar{u}_L u_L \to N_\lambda' N_\lambda} + I_{N_\lambda}^+ \mathcal{M}_{\text{Born}}^{\bar{d}_L d_L \to W_\lambda^+ W_\lambda^-} \right) \log\left(\frac{|\hat{t}|}{\hat{s}}\right) \right.$$

$$\left. - \left(\sum_{N_\lambda'} I_{N_\lambda'}^+ \mathcal{M}_{\text{Born}}^{\bar{d}_L d_L \to N_\lambda' N_\lambda} + I_{N_\lambda}^+ \mathcal{M}_{\text{Born}}^{\bar{u}_L u_L \to W_\lambda^+ W_\lambda^-} \right) \log\left(\frac{|\hat{u}|}{\hat{s}}\right) \right] \right\} \left(\mathcal{M}_{\text{Born}}^{\bar{d}_L u_L \to W_\lambda^+ N_\lambda} \right)^{-1}.$$

$$\text{(A.18)}$$

In the cases $\lambda = L$ and $\lambda = T$, the sums run over $N_L' = \chi, H$ and $N_T' = A, Z$, respectively, and $I_{N_\lambda}^+$ are defined in (B.23) and (B.27) of Ref. [22]. Using the SU(2)-transformed Born matrix elements given in (A.7) and (A.8), we obtain

$$\delta_{\bar{d}_L u_L \to W_L^+ Z_L}^{\text{SSC}} = -\frac{\alpha}{2\pi} \frac{1}{s_W^2} \log\left(\frac{\hat{s}}{M_W^2}\right) \left[\log\left(\frac{|\hat{u}|}{\hat{s}}\right) + \log\left(\frac{|\hat{t}|}{\hat{s}}\right) - \frac{s_W^2}{c_W^2} Y_{q_L} \log\left(\frac{|\hat{t}|}{|\hat{u}|}\right) \right]$$

$$+ 2l^{\text{em}}(M_W^2) \left[Q_d \log\left(\frac{|\hat{t}|}{\hat{s}}\right) - Q_u \log\left(\frac{|\hat{u}|}{\hat{s}}\right) \right],$$

$$\delta_{\bar{d}_L u_L \to W_T^+ N_T}^{\text{SSC}} = -\frac{\alpha}{2\pi} \frac{1}{s_W^2} \log\left(\frac{\hat{s}}{M_W^2}\right) \left[\log\left(\frac{|\hat{t}|}{\hat{s}}\right) + \log\left(\frac{|\hat{u}|}{\hat{s}}\right) + G_+^N \log\left(\frac{|\hat{t}|}{|\hat{u}|}\right) \right]$$

$$+ 2l^{\text{em}}(M_W^2) \left[Q_d \log\left(\frac{|\hat{t}|}{\hat{s}}\right) - Q_u \log\left(\frac{|\hat{u}|}{\hat{s}}\right) \right], \quad \text{(A.19)}$$

where

$$l^{\text{em}}(M^2) = \frac{\alpha}{4\pi} \left[\frac{1}{2} \log\left(\frac{M_W^2}{M^2}\right) + \log\left(\frac{M_W^2}{\lambda^2}\right) \right], \quad \text{(A.20)}$$

and G_+^N is given in (A.16).

A.5 Single-logarithmic corrections

The single-logarithmic corrections consist of the contributions δ^C and δ^{PR} described in Sect. A.1. For longitudinally polarized final states, according to Eqs. (4.6) and (4.33) in Ref. [13], the corrections δ^C read

$$\delta_{\bar{d}_L u_L \to W_L^+ Z_L}^C = \frac{\alpha}{4\pi} \left[\left(3C_{q_L}^{\text{ew}} + 4C_\Phi^{\text{ew}} \right) \log\left(\frac{\hat{s}}{M_W^2}\right) - \frac{3}{2s_W^2} \frac{m_t^2}{M_W^2} \log\left(\frac{\hat{s}}{m_t^2}\right) \right]$$

$$+ \sum_{\varphi=\bar{d}_L, u_L, W^-} Q_\varphi^2 l^{\text{em}}(m_\varphi^2), \quad \text{(A.21)}$$

and the parameter renormalization yields

$$\delta_{\bar{d}_L u_L \to W_L^+ Z_L}^{\text{PR}} = -\frac{\alpha}{4\pi} b_W^{\text{ew}} \log\left(\frac{\hat{s}}{M_W^2}\right) + \Delta\alpha(M_W^2), \quad \text{(A.22)}$$

where $b_W^{\rm ew} = 19/(6s_{\rm w}^2)$ is the one-loop coefficient of the SU(2) β-function, and $\Delta\alpha(M_{\rm W}^2)$ represents the running of the electromagnetic coupling constant from the scale 0 to $M_{\rm W}$.

If the final-state gauge bosons are transversely polarized then the $\log{(\hat{s}/M_{\rm W}^2)}$ contributions in $\delta^{\rm C}$ which are associated to the final gauge bosons cancel the $\log{(\hat{s}/M_{\rm W}^2)}$ contributions originating from parameter renormalization, and according to Eqs. (4.6) and an analogue of (A.11) in Ref. [13] one obtains

$$
\delta^{\rm C}_{\bar{\rm d}_{\rm L}{\rm u}_{\rm L}\to{\rm W}_{\rm T}^+ N_{\rm T}} + \delta^{\rm PR}_{\bar{\rm d}_{\rm L}{\rm u}_{\rm L}\to{\rm W}_{\rm T}^+ N_{\rm T}} =
$$
$$
= \frac{3\alpha}{4\pi} C_{q_{\rm L}}^{\rm ew} \log\left(\frac{\hat{s}}{M_{\rm W}^2}\right) + \sum_{\varphi=\bar{\rm d}_{\rm L},{\rm u}_{\rm L},{\rm W}^-} Q_\varphi^2 l^{\rm em}(m_\varphi^2) + \frac{1}{2}(1+\delta_{N{\rm Z}})\Delta\alpha(M_{\rm W}^2), \quad\text{(A.23)}
$$

where $\delta_{N{\rm Z}}$ represents the Kronecker symbol.

References

[1] K. T. Matchev and D. M. Pierce, Phys. Rev. D **60** (1999) 075004 [hep-ph/9904282]; Phys. Lett. B **467** (1999) 225 [hep-ph/9907505].

[2] J. Bagger *et al.*, Phys. Rev. D **49** (1994) 1246 [hep-ph/9306256]; Phys. Rev. D **52** (1995) 3878 [hep-ph/9504426].

[3] S. Haywood, P. R. Hobson, W. Hollik, Z. Kunszt *et al.*, hep-ph/0003275, in *Standard Model Physics (and more) at the LHC*, eds. G. Altarelli and M. L. Mangano, (CERN-2000-004, Genève, 2000) p. 117.

[4] L. Dixon, Z. Kunszt and A. Signer, Phys. Rev. D **60** (1999) 114037 [hep-ph/9907305].

[5] D. De Florian and A. Signer, Eur. Phys. J. C **16** (2000) 105 [hep-ph/0002138].

[6] J. M. Campbell and R. K. Ellis, Phys. Rev. D **60** (1999) 113006 [hep-ph/9905386].

[7] J. Ohnemus, Phys. Rev. D **44** (1991) 3477.

[8] S. Frixione, P. Nason and G. Ridolfi, Nucl. Phys. B **383** (1992) 3.

[9] U. Baur, T. Han and J. Ohnemus, Phys. Rev. D **51** (1995) 3381 [hep-ph/9410266].

[10] U. Baur, S. Keller and D. Wackeroth, Phys. Rev. D **59** (1999) 013002 [hep-ph/9807417]; U. Baur and D. Wackeroth, hep-ph/0011080; U. Baur, O. Brein, W. Hollik, C. Schappacher and D. Wackeroth, KA-TP-26-2001, hep-ph/0108274; S. Dittmaier and M. Krämer, DESY 01-121, hep-ph/0109062.

[11] W. Beenakker *et al.*, Nucl. Phys. B **410** (1993) 245.

[12] P. Ciafaloni and D. Comelli, Phys. Lett. B **446** (1999) 278 [hep-ph/9809321]; J. H. Kühn, S. Moch, A. A. Penin and V. A. Smirnov, hep-ph/0106298; V. S. Fadin, L. N. Lipatov, A. D. Martin and M. Melles, Phys. Rev. D **61** (2000) 094002 [hep-ph/9910338]; M. Melles, hep-ph/0104232; W. Beenakker and A. Werthenbach, Phys.

Lett. B **489** (2000) 148 [hep-ph/0005316]; M. Beccaria *et al.*, Phys. Rev. D **61** (2000) 073005 [hep-ph/9906319]; J. Layssac and F. M. Renard, Phys. Rev. D **64** (2001) 053018 [hep-ph/0104205].

[13] A. Denner and S. Pozzorini, Eur. Phys. J. C **18** (2001) 461 [hep-ph/0010201].

[14] A. Denner and S. Pozzorini, Eur. Phys. J. C **21** (2001) 63 [hep-ph/0104127].

[15] F. Abe *et al.* (CDF Collaboration), Phys. Rev. Lett. **75** (1995) 1017; F. Abachi *et al.* (D0 Collaboration), Phys. Rev. Lett. **77** (1996) 3301; Phys. Rev. Lett. **79** (1997) 1441.

[16] A. Ballestrero, hep-ph/9911318.

[17] A. Ballestrero and E. Maina, Phys. Lett. **B350** (1995) 225 [hep-ph/9403244].

[18] H. L. Lai *et al.* (CTEQ Collaboration), Eur. Phys. J. **C12** (2000) 375-392 [hep-ph/9903282].

[19] W. Beenakker, F. A. Berends and A. P. Chapovsky, Nucl. Phys. B **548** (1999) 3 [hep-ph/9811481].

[20] A. Denner, S. Dittmaier, M. Roth and D. Wackeroth, Nucl. Phys. B **587** (2000) 67 [hep-ph/0006307].

[21] S. Jadach, W. Placzek, M. Skrzypek, B. F. Ward and Z. Was, hep-ph/0007012.

[22] W. Beenakker, A. P. Chapovsky and F. A. Berends, Phys. Lett. B **411** (1997) 203 [hep-ph/9706339]; Nucl. Phys. B **508** (1997) 17 [hep-ph/9707326].

[23] A. Denner, S. Dittmaier and M. Roth, Nucl. Phys. B **519** (1998) 39 [hep-ph/9710521]; Phys. Lett. B **429** (1998) 145 [hep-ph/9803306].

[24] M. Beccaria, F. M. Renard and C. Verzegnassi, hep-ph/0103335.

[25] J. Gunion, Z. Kunszt and M. Soldate, Phys. Lett. **163B** (1985) 389; J. Gunion and M. Soldate, Phys. Rev. **D34** (1986) 826; W. J. Stirling *et al.*, Phys. Lett. **163B** (1985) 261.

[26] U. Baur, S. Errede and G. Landsberg, Phys. Rev. D **50** (1994) 1917 [hep-ph/9402282].

[27] S. Pozzorini, *Dissertation Universität Zürich, 2001*.